

Hadronic structure on the light-front I

Instanton effects and quark-antiquark effective potentials

Edward Shuryak* and Ismail Zahed†

Center for Nuclear Theory, Department of Physics and Astronomy,
Stony Brook University, Stony Brook, New York 11794-3800, USA

This is the first of a sequence of papers that address the non-perturbative origin of the central, and spin-dependent forces between quarks. Its main thrust is a focus on meson spectroscopy in the center of mass frame. We suggest a novel “dense instanton ensemble” model for the QCD vacuum, to explain the interquark forces in mesons, from quarkonia to heavy-light and light-light ones. The sequels will show how to export these interactions to the light front, and derive the corresponding Hamiltonians, mesonic and baryonic light front wavefunctions. The ultimate aim of the series is to bridge the gap between hadronic spectroscopy and partonic observables.

I. INTRODUCTION

The physics of hadrons is firmly based in Quantum Chromodynamics, a theory over half a century old. One might think that by now this subject has reached a solid degree of maturity with most issues settled. Unfortunately this is not yet the case. The field of non-perturbative QCD consists of several subfields, which can be defined as follows:

1. *hadronic spectroscopy* (masses and wave functions of mesons, baryons, pentaquarks, etc);
2. *QCD vacuum structure* (vacuum condensates, Euclidean correlation functions, etc);
3. *light-front observables* (distributions amplitudes, parton distribution functions or PDFs, etc).

They are relatively weakly connected, although in the past decade considerable efforts to bridge them has taken place. Our set of papers is another effort in this direction. In this introductory section we will give a brief description of the two aforementioned subfields. The third one will be discussed in the papers to follow.

A. Hadronic structure

This field originated in the early 1960’s, and experienced a rapid expansion in the last decade, due to the discoveries of multi-quark hadrons in the heavy-light sector. We will not discuss these “exotic hadrons” in this work but focus on the underlying physics at the origin of the inter-quark forces. Parameterizing and understanding them is a needed

step, setting the stage for derivation of the effective Hamiltonians on the light front.

Early nonrelativistic quark models achieved resounding success, in part through simple formulae for the masses and magnetic moments of baryons made of light quarks. The revolutionary discoveries of 1970’s of “quarkonia”, the bound states made of heavy c, b quarks, revealed families of narrow bound states well described by the celebrated Cornell potential

$$V_{\text{Cornell}}(r) = -\frac{4\alpha_s}{3} \frac{1}{r} + \sigma_T r \quad (1)$$

Further theory effort developed effective non-relativistic theories, such as non-relativistic QCD (NRQCD) and perturbative non-relativistic QCD (pNRQCD). They put spectroscopy of quarkonia close to that of atoms and nuclei in accuracy. A number of *universal* (flavor independent) central and spin-dependent potentials were defined, expressed *via* certain nonlocal correlators of vacuum gauge fields. For short but concise summary see e.g. [1].

The Cornell potential attributes the short-distance potential to perturbative one-gluon exchange, and its large distance $\mathcal{O}(r)$ contribution to the tension of the confining flux tube (QCD string). The issues to be discussed in this paper are the non-perturbative origins of the inter-quark interaction at *intermediate* distances $r \sim 0.2 - 0.5$ fm. Those are especially important for small size-hadrons, such as bottomonia or pions (see below).

A static quark potential $V_C(r)$ is defined through a vacuum average of a pair of parallel Wilson lines,

$$e^{-V_C(r)T} = \langle W(\vec{x}_1)W^\dagger(\vec{x}_2) \rangle \quad (2)$$

* edward.shuryak@stonybrook.edu

† ismail.zahed@stonybrook.edu

defined by

$$W(\vec{x}) = \text{Pexp} \left(ig \int_W dx_4 A_\mu^a(x_4, \vec{x}) \hat{T}^a \right) \quad (3)$$

where color generator $\hat{T}^a = t^a/2$, with t^a Gell-Mann matrices. $t\text{Pexp}$ is path-ordered matrix product. The parallel lines are running in the Euclidean time direction, separated by the spatial distance $r = |\vec{x}_1 - \vec{x}_2|$. The lines are connected at times $\pm T/2$, but eventually the limit of large time $T \rightarrow \infty$ is assumed, this is mostly unimportant. Historically, the derivation of this potential has been at the forefront of lattice studies of the QCD vacuum. In a way, it is similar in spirit to the Born-Oppenheimer approximation in molecular physics, where the probe quarks back-reaction is ignored. For recent developments and references, we refer to the work by Brambilla et al [2].

Traditionally, the central potential was used as linear $V_c(r) = \sigma_T r$ with σ_T be the tension of the confining flux tube (known also as QCD string). So, one might think the issue of the central potential is very simple. Unfortunately, it is far from being so, and there are several impediments for usage of the flux tubes.

The first is that the simple linear term is expected to be correct at large distances only, while at smaller r there are other nonperturbative effects as well. The simplest corrections are due to quantum vibrations of the flux tube. The first of them is the famous ‘‘Lusher term’’, attractive $\sim 1/r$. If the string is described by a Nambu-Goto geometrical action, these vibrations are summed up in the so called Arvis form [3]

$$E(r) = \sigma_T r \sqrt{1 - \frac{\pi}{6} \frac{1}{\sigma_T r^2}} \quad (4)$$

This expression predicts that potential vanishes at $r \approx 1/3$ fm. Furthermore, the QCD string may have much more complicated action, so the Arvis potential cannot be really trusted when the corrections are large. Yet the two first expansion terms are universal, see more in [4]. Lattice studies of these corrections (e.g. [5]) in the setting with two static charges, or a flux tube wrapped around the lattice, do confirm these two terms.

Important issue to be discussed is the derivation of the relativistic corrections $\sim (v/c)^2 \sim (\Lambda_{QCD}/m_Q)^2$ where m_Q is heavy quark mass and Λ_{QCD} stands for a ‘‘QCD scale’’. Such perturbative terms are well

known in atomic and nuclear physics, and changing from one-photon to one-gluons exchange is simple. So it is clear how *spin-spin*, *spin-orbit* and *tensor force* V_{SS}, V_{SL}, V_T arise from perturbative contributions, being all just certain derivatives of the Coulomb potential.

The question is what is the nonperturbative contributions to these potentials. Those can be related to Wilson lines decorated by two extra field strengths [6, 7]. Schematically, they have the form

$$\langle W G_{\mu\nu}(x) W W^\dagger G_{\mu\nu}(y) W^\dagger \rangle$$

More details of the invariant spin potentials given in section B.

In a nonrelativistic setting, spin-dependent forces originate from quark (gluo)-magnetic moments interacting with vacuum fluctuations of (mostly) *gluomagnetic* fields. Unfortunately, the QCD flux tubes carry *electric* flux: models of their structure and lattice studies specify mostly distribution of the gluoelectric fields in them, not the gluo-magnetic ones needed for the spin forces. So, one has to think about other origins of those in the vacuum.

In principle, the pertinent correlation functions can be calculated on the lattice, so one might think that all spin-dependent forces are by now well documented and their origins explained. Unfortunately, this is not the case as quantitative lattice studies have only started recently. Below we will investigate to what extent such correlators, evaluated using certain models of vacuum fields, can reproduce the observed spin-dependent potentials. We will find that in heavy quarkonia instanton-induced forces can provide contributions to perturbative ones, leading together to a good description of splittings for a number of the low-lying states.

However, for spin splittings in light quark states these forces coming from Wilson lines are not sufficient. The resolution comes from additional terms in the quark propagator, related to their disappearance/creation in/from the Dirac sea technically described by parts of the propagators related to *fermionic zero modes*. In other words, there are spin forces induced by ’t Hooft effective Lagrangian for light quarks. In Fig.1 we show schematically how these vertices contribute to the pion and rho meson.

B. QCD vacuum and Instanton Liquid Model

Nonperturbative physics of strong interactions started before the development of QCD in 1970’s.

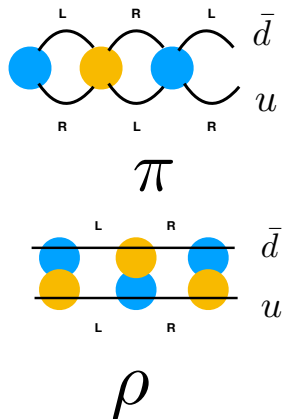


FIG. 1. Schematic representation of the role of instanton-induced 't Hooft Lagrangian in the structure of the pion (upper) and rho meson (lower plot).

Nambu and Jona-Lasinio (NJL) [8], inspired by BCS theory of superconductivity, have qualitatively explained that strong enough attraction of quarks can break $SU(N_f)_A$ chiral symmetry spontaneously and, among many other effects, create near-massless pions. Chiral effective Lagrangians and related theory have lead to one important input, a nonzero *quark condensate* $\langle \bar{q}q \rangle \neq 0$.

The discussion of the “QCD vacuum structure” started with the QCD sum rules [9], where the short-distance description of *Euclidean point-to-point correlation functions* via the Operator Product Expansion (OPE) was related to their long-distance description in terms of the lightest hadrons. The (Euclidean) correlators of QCD operators were calculated in terms of the leading *vacuum condensates*, $\langle G^2 \rangle$, $\langle \bar{q}q \rangle$, etc. Yet it was soon realized that the strongest nonperturbative effects (in the scalar and pseudoscalar channels) are *not* described by the “mean field” OPE predictions [10].

Extensive studies of point-to-point (Euclidean) correlation functions in multiple mesonic channels, based on phenomenology [11], have indeed found striking differences between correlators of operators with different quantum numbers. While for vector currents ($\bar{q}\gamma_\mu q$) made of *light* quarks $q = u, d, s$ only small deviations from free quark propagation is observed, correlators of the scalar and pseudoscalar operators ($\gamma_\mu \rightarrow 1, \gamma_5$) show strong splittings from them at surprisingly small distances. As shown in detail in [11], these splittings found their explanation in terms of topological fluctuations of gluonic

fields, described semiclassically by instantons [12].

The semiclassical model of the QCD vacuum structure based on instantons [13] is known as the “instanton liquid model” (ILM). It introduced an important scale parameter of the nonperturbative vacuum – the typical instanton size

$$\rho \sim \frac{1}{3} \text{ fm} \quad (5)$$

Because it is rather small compared to sizes of most hadrons (except for the lowest Υ s and the pion, see below), where possible we will use a *quasi-local* approximation in which it is going to zero.

In the ILM the vacuum fields are very inhomogeneous: blobs of strong gauge fields (at the instanton centers) surrounded by “empty” space-time, free from nonperturbative fields. Since mid-1990s such field distributions were obtained from lattice configurations by means of various “cooling” methods. A picture is better than many words: so we reproduce in Fig. 2 one visualization of the topological charge distribution from [14–16] which reveals a number of instantons and anti-instantons.

Note that the topological clusters are also threaded by thin center vortices or Z_3 -fluxed strings, which span world-sheet surfaces in 4-dimensions. While the center vortices are important for enforcing confinement at long distances, Fig. 2 shows that they are on average decoupled from the inhomogeneous and strong topological fields. Moreover, their field strength in the vicinity of these topological fields is about $\sigma_T \bar{\rho} \approx 0.3 \text{ GeV}$, which is weaker than the typical chromo-electric or chromo-magnetic field in the instanton center $\sqrt{E} = \sqrt{B} \approx 2.5/\bar{\rho} \approx 1.5 \text{ GeV}$, but crucial for long-distance color correlations.

Instantons are not just semiclassical solitons made of glue. As discovered by 't Hooft [18], they generate 4-dimensional fermionic zero modes which lead to multifermion effective Lagrangian. The instanton-induced 4-quark not only solves the famous “ $U_A(1)$ problem” – by making the η' non-Goldstone and heavy – but it also produces a strong attraction in the σ and π channels. Including those in the framework of the ILM [19] one gets a microscopic understanding of chiral symmetry breaking, chiral perturbation theory, the pion properties etc. 'T Hooft instanton-induced effective Lagrangian is a QCD substitute to the hypothetical Nambu-Jona-Lasinio [8] four-quark interaction.

Another version of this theory look at quarks “hopping” from one instanton to another. The resulting loops in the quark determinant can be ei-

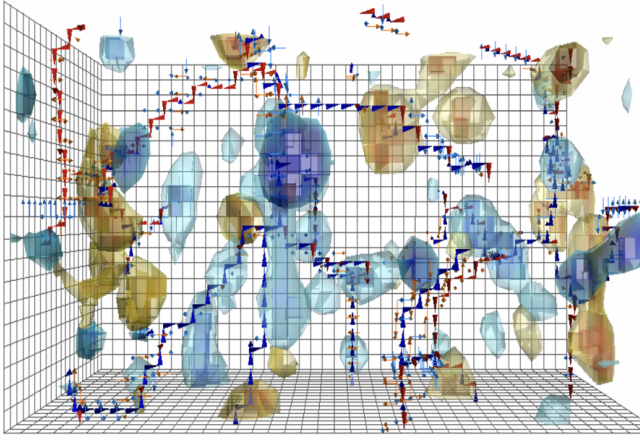


FIG. 2. Instantons (yellow) and anti-instantons (blue) configurations in the “deep-cooled” Yang-Mills vacuum. After center projection, they are threaded by center P-vortices [15, 16]. They constitute the primordial gluon epoxy (hard glue) at the origin of the light hadron masses [17]. The center P-vortices are responsible for confinement. See text.

ther short or long (infinite in thermodynamic limit $V_4 \rightarrow \infty$). The latter component is responsible for the localization of the Dirac eigenvalues close to zero $\lambda \sim 1/V_4$,

Two parameters of the original ILM are the size and the density of instantons

$$\rho = \frac{1}{3} \text{ fm}, \quad n_{I+\bar{I}} = \frac{1}{R^4} = 1 \text{ fm}^{-4} \quad (6)$$

which in turn defines the so called *diluteness parameter*

$$\kappa \equiv \pi^2 \rho^4 n_{I+\bar{I}} \quad (7)$$

So, the ILM predicts it to be small $\kappa_{\text{ILM}} \sim \mathcal{O}(1/10) \ll 1$. These parameters have withstood the scrutiny of time, and describe rather well the chiral dynamics related to pions, the Euclidean correlation functions in the few femtometers range, and much more, see [20] for a review.

Another formulation of chiral symmetry breaking relates it to the *collectivization* of the instanton zero modes, into the so-called “zero mode zone” (ZMZ). Due to nonzero matrix elements of the Dirac operator, near-zero Dirac eigenvalues are residing within

a strip of small width

$$|\lambda| \sim \text{width (ZMZ)} \sim \frac{\rho^2}{R^3} \sim 20 \text{ MeV} \quad (8)$$

as predicted by the original ILM with the parameters given above (6). In [21] the meson and baryon spectroscopy was studied, with all Dirac states inside a certain strip of eigenvalues $|\lambda| < \Delta$ eliminated. A strong restructuring of the light hadronic spectra was indeed observed if $\Delta > \text{width (ZMZ)}$. In particular, the Nambu-Goldstone modes (pions) totally disappear from the spectra, as expected. It would be interesting to extend the same analysis to the heavy-light sectors, and to address more generally what happens with all forms of spin-dependent forces.

Further statistical description of interacting instanton ensembles was developed by mean field methods and statistical simulations, for review see [20]. Some related lattice studies are [22, 23].

C. Topological landscape and $I\bar{I}$ molecules

The “landscape” refers to the *minimal energy* gauge field configurations, as a function of two main variables. The first is the topological Chern-Simons number

$$N_{CS} \equiv \frac{\epsilon^{\alpha\beta\gamma}}{16\pi^2} \int d^3x \left(A_\alpha^a \partial_\beta A_\gamma^a + \frac{1}{3} \epsilon^{abc} A_\alpha^a A_\beta^b A_\gamma^c \right) \quad (9)$$

For the second we will use the r.m.s. size of the configuration, related to the field strength

$$\rho_{r.m.s.} = \frac{\int r^2 G^2 d^3r}{\int G^2 d^3r} \quad (10)$$

For fixed ρ , the landscape is shown in Fig.3. It has been defined in Ref [24] and is given in a parametric form

$$U_{\min}(k, \rho) = (1 - k^2)^2 \frac{3\pi^2}{g^2 \rho} \quad (11)$$

$$N_{CS}(\kappa) = \frac{1}{4} \text{sign}(k) (1 - |k|)^2 (2 + |k|)$$

with parameter κ . At $\kappa = \pm 1$ the minimal energy is zero, while $k = 0$ corresponds to a maximum of the energy. This point was called “the sphaleron” in electroweak theory [25]. The set of configurations at arbitrary κ is called the *sphaleron path*. Those consist of static 3d magnetic field configurations, known also as the *turning points* (by analogy to points in quantum mechanics where the semiclassical momentum vanishes).

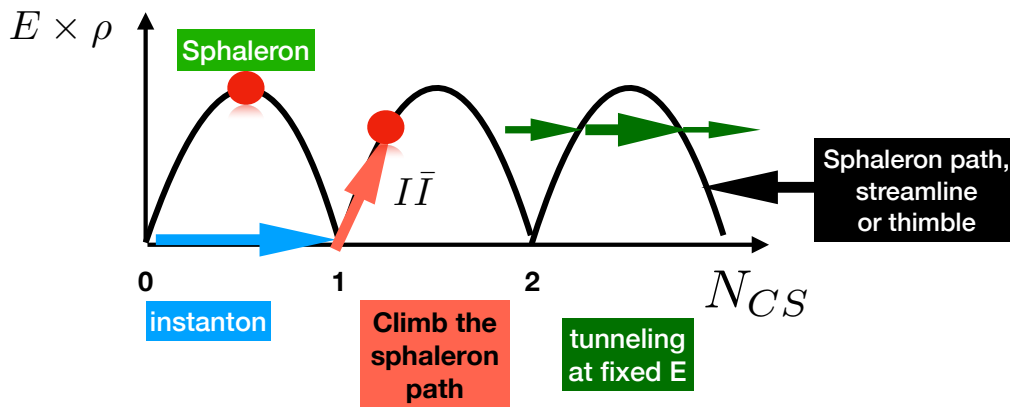


FIG. 3. The topological landscape: minimal energy (times r.m.s. size) versus Chern-Simons number N_{CS} (left); thimble path (center); tunneling at nonzero energy (right).

The (anti)instanton is a tunneling path connecting the *bottoms* of two subsequent valleys, at energy zero. Since they have topological charge $Q = \pm 1$, they result in change of Chern-Simons number $\Delta N_{CS} = \pm 1$.

However instanton paths are *not the only form of topological fluctuations* which may occur in this landscape. Indeed, we will discuss *two* additional sets of paths: (i) those that travel the landscape along the sphaleron path (or ‘streamline’); (ii) those that travel the landscape at fixed energy, including the tunneling; all of which are illustrated in Fig. 3

The first set is described by a constrained Yang-Mills equation with a nonzero r.h.s., or external current, which drags them up (or down) the potential along the gradient. In the mathematical literature this construction is known as “Lefschetz thimbles”, a special path connecting two extrema of a function following its gradient. In QCD-related literature they are known as “streamline” configurations described by overlapping instanton-antiinstanton pairs or molecules.

The second set is described by Yang-Mills equation with a *zero* r.h.s., and thus is occurring at fixed energy. The path’s history passes the “turning points” *twice*, with Euclidean time solution in between them, known as *tunneling at nonzero energy*. In general, those should be complemented by Minkowskian time solutions, before and after turning points. Technical name for those is “*zigzag path*” indicating a turn from real to imaginary time and

then back to real.

Both sets of solutions, with proper references, we detail in the Appendices. What we would like to emphasize here is the fact that they describe gauge field fluctuations *different from* well separated instantons. They are neither self-dual nor possess (near) zero Dirac eigenvalues – and therefore they do not contribute to chiral symmetry breaking and were not included in the original ILM. And still, they do describe certain fluctuations of vacuum gauge fields, and therefore can contribute to certain observables: especially the Wilson lines. Therefore, we will investigate their contributions to central and spin-dependent forces between quarks. The inclusion of “molecules” or “zigzag paths” is the novel element of novel vacuum model we develop here.

Close instanton-antiinstanton pairs are of course known, and in particular there were observed on the lattice. They are however not seen in Fig. 2 obtained by so called “deep cooling” of configurations, during which close instanton-antiinstanton pairs are already annihilated. The application of the “molecular component” of the vacuum was made previously in connection to phase transitions in hot/dense matter. Indeed, (if quark masses are neglected) this component is the only one which survives at temperatures $T > T_c$, where chiral symmetry is restored. Account for “atomic” and “molecular” components together started with [26]. The “molecular component” was also shown to be important at high baryonic densities, where it contributes to quark pairing and color

superconductivity [27]. More recently, we have explored it in the context through non-perturbative contributions to the mesonic form factors [28] and matching kernels [29].

The theory of sphaleron processes (sketched in the middle of Fig.3. is related to the issue of $I\bar{I}$ interaction. Numerical calculation of the “streamline” along the action gradient was first done for quantum-mechanical instantons in [30], for gauge theory the “streamline equation was derived in [31], solved approximately by [32] and numerically by [33]. The surprising finding of the latter paper was that “Yung ansatz” was rather accurate not only at large distances $R \gg \rho$ between instanton and antiinstanton, where it was derived, but in fact for any distance till zero. Note that the last two papers used conformal inversion at the center of the instanton, making I and \bar{I} co-central.

Consider I and \bar{I} of the same size ρ and same color orientation, with 4-distance between their centers R serving as the parameter of the set, with $x_{1\mu} = (0, 0, 0, R/2), x_{2\mu} = (0, 0, 0, -R/2)$. In the mathematical literature such set is known as *Lefschets thimble*, it connects one extremum at large R , the independent I and \bar{I} , with another, the zero field at $R = 0$. Note that at the locations $y_4 < 0$ the gauge fields are approximately antiselfdual $\vec{E} \approx -\vec{B}$, and at $y_4 > 0$ they are approximately selfdual $\vec{E} \approx \vec{B}$. At $y_4 = 0$ the electric field vanishes. As shown in [24], these 3d magnetic objects obtained using Yung ansatz are very close to the sphaleron path configurations obtained by constrained energy minimization.

The instanton-antiinstanton streamline therefore provides a semiclassical description of the sphaleron production. In the context of electroweak theory it was first used in [34] and [35] three decades ago. Recent interest in the production of QCD sphalerons at LHC and RHIC colliders is discussed in our recent paper [36].

Let us now move to lattice observables, to which the “molecular component” of the instanton ensemble contributes. The simplest of which is the so called *gluon condensate* $\langle G_{\mu\nu}^2 \rangle$ introduced in the context of the QCD sum rules framework [9]. The accuracy of this number was later questioned and it was revised to a larger value. Further discrepancies were shown in lattice studies, that were attempting to extract local (or nonlocal) observables with powers of the gauge field strength $G_{\mu\nu}$.

Nowadays, when “cooling” by the gradient flow

method can be consistently related to the renormalization group (RG) flow [37], one can put the appropriate scale dependence of the “molecular component” on a firm basis. Skipping several decades, let us take as an example the recent work [38] which studies the 3- and 4-point gluon field correlators and related their evolution to topology during cooling. Their original motivation was to extract the gluon coupling $\alpha_s(k)$, so the observable was chosen to be the ratio of the 3-point to 2-point Green function leading to effective coupling

$$\alpha_{MOM}(k) = \frac{k^6 \langle G^{(3)}(k^2) \rangle^2}{4\pi \langle G^{(2)}(k^2) \rangle^3} \quad (12)$$

In the “uncooled” quantum vacuum (with gluons) the effective coupling starts running downward at large $k > 1 \text{ GeV}$, as expected by asymptotic freedom. However at low $k \rightarrow 0$, one finds another persisting positive power of k , with a slope that matches exactly the one following from an instanton ensemble [39]

$$\alpha_{MOM}(k) \rightarrow \frac{k^4}{18\pi n_{I+\bar{I}}} \quad (13)$$

Furthermore, it was observed that with increasing cooling time τ , the same power spreads to higher momenta, $k > 1 \text{ GeV}$. It was observed that “cooling” eliminates not only perturbative gluons, but close instanton-antiinstanton pairs as well.

The dependence of the mean instanton sizes and density as a function of the (gradient flow) cooling time is shown in Fig.4, from [38]. Their main conclusion from this analysis was that the size and density – extrapolated to *zero* cooling time ($\tau \rightarrow 0$) – are

$$\rho \rightarrow \frac{1}{3} \text{ fm}, \quad n \rightarrow 10 \text{ fm}^{-4} \quad (14)$$

Therefore one can see that total instanton density is significantly larger than known before from “deep cooling” (large τ) of $1/\text{fm}^4$, as in the original ILM. In fact, the density may even be larger than that, because the definition of instantons used in this paper exclude pairs (“molecules”) which are too close. We will use these numbers, as indicative, for our “dense instanton liquid model” below.

D. Content of this paper

In section II we will argue that the *upper* limit on the total instanton density can be deduced from

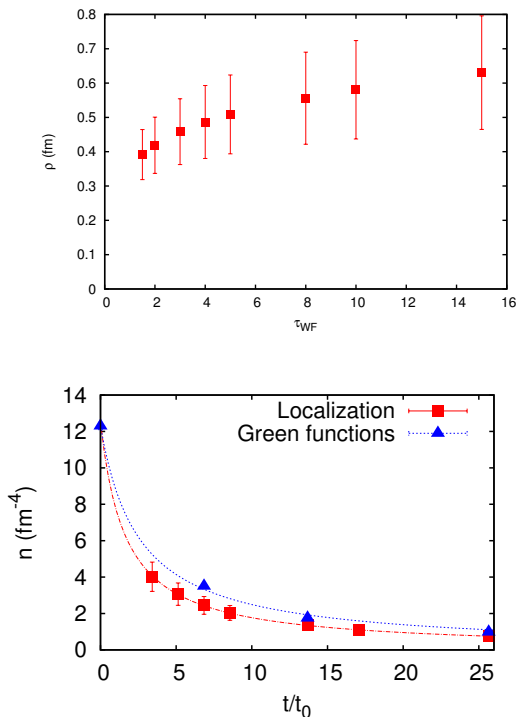


FIG. 4. The dependence of the mean instanton sizes (upper plot) and density (lower plot) on the gradient flow cooling time τ (arbitrary units). The quantum vacuum of course corresponds to an extrapolation to $\tau \rightarrow 0$.

known magnitude of the central potentials, e.g. from quarkonium spectroscopy.

The main purpose of the present paper is to quantify *nonperturbative spin-dependent* forces. We begin by reviewing their phenomenology in section III A and then the theory in III D which is based on the standard "Wilson line plus two field strengths" correlators. The contribution of an instanton to a pair of Wilson lines can be readily calculated analytically. This approach has been first used to calculate the static $\bar{Q}Q$ potential by the original Princeton group [6]. Two decades later we generalized it to high energy $\bar{Q}Q$ and dipole-dipole scatterings [40]. In the scattering approach, the Wilson lines are first assumed to cross at an angle θ_{12} in Euclidean geometry. The final result is analytically transformed to a scattering amplitude (near) the light front by the substitution of the angle θ_{12} between two Wilson lines, to the hyperbolic angle iy with *relative rapidity* y between two colliding particles in the ultra-relativistic limit. Unfortunately, neither of these

works were widely noticed or actually used by phenomenologists (except for [41, 42]).

An extensive study of the instanton-induced effects on heavy quarkonia has been revived recently by Musakhanov et al (see e.g. [43]), who calculated the magnitude of the effect for the central as well as the spin-spin, spin-orbit and tensor forces. Using the original ILM parameters of [44], it was found that the central potential is of magnitude ~ 150 MeV at large r , a relatively small correction to the phenomenological potential. The spin-spin potential was also calculated, and was found to be short ranged and of order of about 30 MeV, also a small correction. The spin-orbit and tensor forces are even smaller.

We will modify these results by using our new model for the instanton ensemble, and compare the results to the lattice results for spin-spin forces in section III C, and to the phenomenological vector-pseudoscalar mass splittings in section III D. We will see that in this setting the splittings in heavy-heavy quarkonia are reproduced.

The next challenge using the novel model, is to extend the same analysis to heavy-light mesons such as $B, D\dots$ and eventually light-light mesons. The goal is to find out whether these lighter systems can also be described analogously using variants of the "constituent quark" models.

Not all instanton-induced effects are included using temporal Wilson loops with straight fermion lines. The part of the quark propagation, related to the chiral anomaly, instanton zero modes and the 't Hooft Lagrangian has to be treated separately as we detail in section IV. Only the inclusion of this effective interaction can describe pions.

Yet to get the correct mass and wave function of the vector (ρ) mesons, we also need the effective forces originating from $I\bar{I}$ molecules, see IV E. The discussion of the heavy-light systems is in section IV F. The conclusions reached in this study are summarized in section V.

II. CENTRAL POTENTIALS

A. Flux tubes vs the instantons

The static quark potential $V_C(r)$ is defined via the vacuum average of the *Wilson line*

$$W = \text{Pexp}\left[ig \int dx^\mu A_\mu^a \hat{T}^a\right] \quad (15)$$

over a closed rectangle $r \times T$. In the limit when the time extent is much larger than the spacial extent $T \gg r$, one can ignore the small integrals over the spatial direction $r = |\vec{x}_1 - \vec{x}_2|$, and keep only two over the Euclidean time direction, defining the potential by

$$e^{-V_C(r)T} = \langle W(\vec{x}_1)W^+(\vec{x}_2) \rangle \quad (16)$$

For decades this Wilson's definition is used in lattice studies.

We already noted that due to quantum vibrations of the QCD string, the flux tube contribution to $V_C(r)$ is in fact rather uncertain at the distance scale $\sim 1/3 \text{ fm}$. Yet precisely this distance range happens to be the most important one for spin-dependent forces.

Another important point is that the quark spins, due to the magnetic moments, interact with *magnetic* fields. The spin-dependent potentials can be defined via the average of two Wilson lines to which either *two magnetic field strengths* or *product*

of electric and magnetic fields are added. The QCD flux tubes description, however, provides a description of the *electric* fields only. Therefore, one might think that they cannot contribute significantly to the spin forces.

The instantons (antiinstantons) are selfdual (anti-selfdual) vacuum fluctuations, in which the modulus of the magnetic and electric fields are equal. Furthermore, the BPTS *instanton* fields have ‘‘hedgehog’’ structure $A_\mu^a \sim \eta_{\mu\nu}^a x^\nu$, and since along the straight line dx^μ is the same vector, the colors are rotated around the same direction. Therefore, the accumulated rotation angle is given by an integral along the line [6, 7]. The instanton-induced central potential has the form

$$V_{\text{instanton}}(r) = \frac{4\pi n_{\bar{I}+I} \rho^3}{N_c \rho} I\left(\frac{r}{\rho}\right) \quad (17)$$

Here $n_{\bar{I}+I}$ is the instanton plus antiinstanton 4-dimensional density, ρ is the typical instanton size, and the function $I(x)$ is defined by an integral over the location of the instanton center y_μ .

$$I(x) = \int_0^\infty dy y^2 \int_{-1}^1 dc \left[1 - \cos(\alpha_1) \cos(\alpha_2) - \frac{y + xc}{\sqrt{y^2 + x^2 + 2xyc}} \sin(\alpha_1) \sin(\alpha_2) \right] \quad (18)$$

in which c is the cosine of the angle between \vec{r} and \vec{y} , going through the instanton center. The two color rotation angles are

$$\alpha_1 = \pi \frac{y}{\sqrt{y^2 + \rho^2}}, \quad \alpha_2 = \pi \sqrt{\frac{y^2 + x^2 + 2xyc}{y^2 + x^2 + 2xyc + \rho^2}} \quad (19)$$

Note that they vanish for zero impact parameter of the line $y = 0$, and become π if their impact parameter gets large. In the former case the integrand above vanishes as $\cos(\alpha) = 1$, in the latter $\cos(\alpha) = -1$ and the integrand is maximal.

Using the instanton parameters of the ILM (6) one finds the large distance value of about 150 MeV [43]. We however extend the original ILM including also a ‘‘molecular $I\bar{I}$ component’’. As a first approximation (to be improved later) we will do so by just enhancing the density, keeping the function with the same instanton size $\rho = 1/3 \text{ fm}$ (as justified by lattice data of Fig.4(a)).

The ‘‘molecular density’’ n_{mol} should be limited from above by the phenomenological value of the central potential. The instanton contribution to $V_C(r)$ is shown in Fig.5 (solid line) for

$$n \equiv n_{\text{mol}} + n_{\text{ILM}} = 7. \text{ fm}^{-4} \quad (20)$$

Note that this density is about twice lower than indicated by a triangle and extrapolation lines in Fig.4(b).

If so, the instanton-induced central potential gets quite close to the phenomenologically known one, for intermediate distances $r < 3 \text{ GeV}^{-1}$. Assuming it is indeed the case, we proceed to calculate the spin-dependent effects below, and will show that the results are quite reasonable.

Note further that with this choice, the diluteness parameter $\kappa \approx 1$. In other words, the ensemble is very dense, with the mean interparticle distance as low as

$$R_{\text{dense}} \equiv n^{-1/4} = 0.61 \text{ fm} \approx 2\rho$$

(It may appear too dense: but remember that the $I\bar{I}$ molecules are not in fact two independent instantons, and their fields and action are partially cancelling each other.)

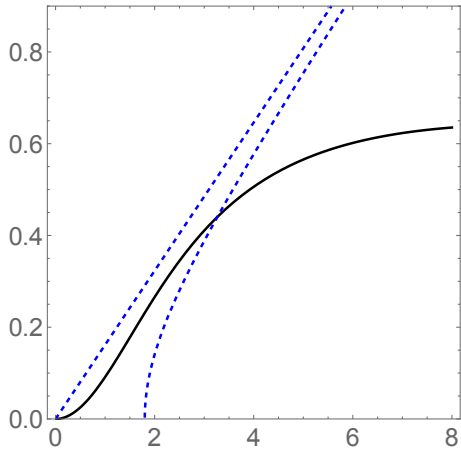


FIG. 5. Comparison of the central potentials $V_C(r)$ versus the inter-quark distance r in GeV^{-1} (so $1 \text{ fm} \approx 5\text{GeV}^{-1}$ on this plot). The solid line is the one derived from the “dense” instanton ensemble. The potential produced by the confining flux tube is illustrated by two blue dashed lines, the upper linear line is the classical string, and the lower is the Arvis potential (4) accounting for quantum string vibrations [3].

But before we do so, let us take a well studied example – the bottomonium states – and check to what extent the difference between the linear and instanton-induced potential at $r > 1 \text{ fm}$ is reflected in the mass spectra. We have calculated the levels of bottomonium $\bar{b}b$ states using both potentials. In Fig.6 we show their non-relativistic energies for four radial excitations, with S -shell, orbital momentum $L = 0$. (As the spin-dependent forces were not included – we return to those in the next subsections – therefore the calculation corresponds to the *spin averaged* combination, of $J = 1$ Upsilon and $J = 0$ η_b states.) The difference between these two potentials at large distances $r > 5 \text{ GeV}^{-1} \approx 1 \text{ fm}$ does indeed translate into different predictions for radially excited states. At large n , the instanton-induced version does not keep with the expected Regge behavior $m_n^2 \sim n$. However, for the select bottomia considered there is little practical difference between the potentials used. (In the matrix elements used for lighter systems below, we will still use the wave functions obtained with the usual Cornell potential.)

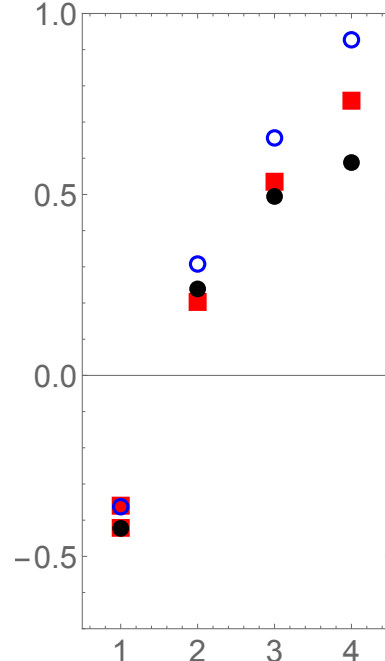


FIG. 6. Nonrelativistic energies $M_i - 2M_b$ for spin averaged $\bar{b}b$ states as a function of the principal quantum number n . Five red squares show the experimentally determined masses of $\Upsilon[1S], \eta_b[1S], \Upsilon[2S], \Upsilon[3S], \Upsilon[4S]$, the blue circles correspond to the standard Cornell potential, while the black closed circles are based on the instanton-induced potential shown in Fig.5.

B. Contributions to V_C of $I\bar{I}$ molecules

We start with $I\bar{I}$ pairs, with a fixed distance R_μ between the centers. The contribution to the central potential strongly depends on the orientation of this vector. When it is lined in time direction, $R_\mu = (0, 0, 0, R)$, as shown in the left of Fig.7, the electric field and potential $\vec{E}(x), A_4(x)$ are time-odd, with the opposite sign between lower and upper subvolumes, the instanton and antiinstanton. Therefore, the color rotation angles in the Wilson lines – integrated over time along the lines with arrows – get contributions of opposite sign which *cancel*. We thus come to the somewhat surprising conclusion that this configuration would *not* contribute to the central potential.

This is not so if R_μ has other orientations, e.g. in one of the space direction. Then the time-oriented Wilson lines would go through either the self-dual or anti-selfdual parts of the “molecule”. At small enough distance between both of them $r < \rho$ they

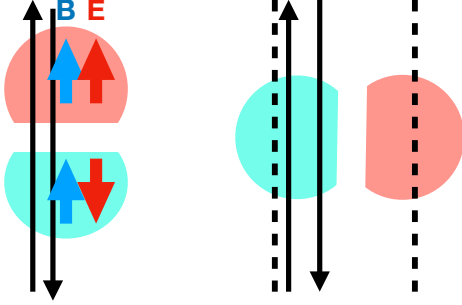


FIG. 7. Instanton-antiinstanton molecule oriented along the time axes (left) and space axes (right).

are likely to go through the same duality, and therefore the result would be qualitatively the same as for a single instanton (discussed in the preceding subsection). At large $r \sim 2\rho$ the opposite would be dominant, with one of the angles in expression (18) changing sign.

C. Fixed energy tunneling events and their contribution to V_C

Tunneling in vacuum in topological landscape proceed at energy zero. But for quarks moving inside hadrons, or during some hadronic reactions, a certain amount of kinetic energy is available. Therefore tunneling through topological barriers may occur not via BPST instanton but with modified tunneling solution, at some nonzero energy. These paths were sketched in the right side of Fig.3: they include two Minkowskian sections of the path, and an Euclidean one. The analytic solutions for a family of such paths, of Yang-Mills equations, can be obtained.

Their Euclidean part interpolates between two “turning point” magnetic configurations. As a re-

sult, the change in Chern-Simons number is fractional. Depending on the energy, one can obtain a single-parameter family of solutions, which interpolate between the bottom of the topological barrier (instanton) and its top (the sphaleron configuration). When analytically continued to Minkowski signature they describe implosion and explosion to and from the magnetic turning points.

Step 1 to obtain such solutions use the $O(4)$ static and symmetric ansatz for the $SU(2)$ configuration in regular gauge

$$A_M^a(y) = 2 \bar{\eta}_{aMN} \frac{y_N}{y^2} f(\xi) \quad (21)$$

with the conformal variable $\xi(y) = \frac{1}{2} \ln(y^2/\rho^2)$. The passage to singular gauge follows from the substitution $f(\xi) \rightarrow f(\xi) - 1$. The corresponding gauge invariant action is

$$S_S = -\frac{1}{4} \int d^4y F_{MN}^a F_{MN}^a \quad (22)$$

or in terms of the conformal variable

$$S_S = 24\pi^2 \int d\xi \left(\frac{f'^2(\xi)}{2} + V(f(\xi)) \right) \quad (23)$$

with the inverted double well potential

$$-V(f) = -2f^2(1-f)^2$$

in Euclidean signature. The $O(4)$ profile $f(\xi)$ extremizes (22) and solves the Jacobi equation

$$\frac{d^2 f}{d\xi^2} = 4(f^2 - f)(2f - 1). \quad (24)$$

The solution to (24) with a sphaleron-like turning point at $\xi = 0$ with zero momentum $f'(\xi = 0) = 0$, is

$$f_k(\xi) = \frac{1}{2} \left(1 + \left(\frac{2k^2}{1+k^2} \right)^{\frac{1}{2}} \operatorname{sn} \left(\xi \left(\frac{2}{1+k^2} \right)^{\frac{1}{2}} - K(k), k \right) \right) \quad (25)$$

with sn the Jacobi sine function. (25) forms a k-family of ξ -periodic functions with the period

$$T_k = 4K(k) \left(\frac{1+k^2}{2} \right)^{\frac{1}{2}} \quad (26)$$

with $K(k)$ the elliptic function.

The solutions (25) carries *energy* (conjugate to ξ -coordinate) at the turning point

$$E_k = \frac{24\pi^2}{\rho} V(f_k(\xi = 0)) = E_0 \left(\frac{1 - k^2}{1 + k^2} \right)^2 \quad (27)$$

with $E_0 = 3\pi^2/\rho$. (27) interpolates continuously between the sphaleron and the instanton for $0 \leq k \leq 1$. At $k = 0$ the energy E_0 is maximal and corresponds to sphaleron mass, the period is $T_0 = \sqrt{2}\pi$ and the profile $f_0(\xi) = \frac{1}{2}$ is constant. At $k = 1$ the instanton energy is $E_1 = 0$, the period $T_1 = \infty$ and the profile is

$$f_1(\xi) = \frac{1}{2} + \frac{1}{2} \operatorname{sn}(\xi - K(1), 1) = \frac{e^{2(\xi - K(1))}}{1 + e^{2(\xi - K(1))}} \quad (28)$$

Note that the argument shift with $K(1)$ in (28), amounts to a rescaling of the instanton size in the conformal coordinate $\rho \rightarrow \rho e^{K(1)}$.

In general, the solution (25) carries Chern-Simons

number N_k as well, that is tied to the energy E_k through the profile of the potential

$$\left(\frac{E_k}{E_0} \right) = 16N_k^2(1 - N_k)^2 \quad (29)$$

with $N_{k=1} = 1$ the instanton topological charge, and $N_{k=0} = \frac{1}{2}$ the sphaleron Chern-Simons number. Only the solution with $N_1 = 1$ is self-dual and stable. All the other sphaleron-like configurations with $N_k < 1$ are unstable extrema. The flavor analogue of these configurations were recently used to construct stable holographic tetraquark states [45, 46].

Step 2 is applying the conformal (stereographic) mapping of the previous solutions that projects the $O(4)$ turning points on the sphere at $\xi^2 = \rho^2$ onto the planar turning point at $t_E = 0$,

$$(x + a)_\mu = \frac{2\rho^2}{(y + a)^2} (y + a)_\mu \quad (30)$$

with $a_\mu = (0, 0, 0, \rho)$. As a result, the gauge fields depend separately on the Euclidean coordinates $t_E = x_4 - Z_4$ and $r = |\vec{x} - \vec{Z}|$ (and parametrically on k).

$$\begin{aligned} A_4^a(t_E, r; k) &= \left(\frac{8\rho t_E x_a}{[(t_E + \rho)^2 + r^2][(t_E - \rho)^2 + r^2]} \right) f_k(\xi_E) \\ A_i^a(t_E, r; k) &= \left(\frac{\delta_{ai}(-t_E^2 - r^2 + \rho^2) + 2\rho\epsilon_{aij}x_j + 2x_i x_a}{[(t_E + \rho)^2 + r^2][(t_E - \rho)^2 + r^2]} \right) 4\rho f_k(\xi_E) \end{aligned} \quad (31)$$

with $Z_\mu = (\vec{Z}, Z_4)$ the collective position, and

$$\xi_E = \frac{1}{2} \ln \left(\frac{(t_E + \rho)^2 + r^2}{(t_E - \rho)^2 + r^2} \right) \quad (32)$$

In Euclidean signature, A_4 and the electric field are real and vanishing at $t_E = 0$ as they should, while A_i and the magnetic field are finite and real. Similar configurations were originally discussed in [47, 48]. The half periodicity (26) maps onto the tunneling time ($r = 0$)

$$\mathcal{T}_k = \rho \left(\frac{e^{\frac{1}{2}T_k} - 1}{e^{\frac{1}{2}T_k} + 1} \right) = \rho \tanh \left(\frac{1}{4}T_k \right) \leq \rho \quad (33)$$

The conformal transforms of the electric and magnetic fields in (D1) are lengthy. The sphaleron configuration with $k = 0$ and $f_0 = \frac{1}{2}$, has $A_4 = 0$ at the

turning point $t_E = 0$, with an $O(3)$ symmetric and well localized squared magnetic field

$$\vec{B}^2(0, r; 0) = \frac{96\rho^4}{(\rho^2 + r^2)^4} \quad (34)$$

When analytically continued to Minkowski signature $t_E \rightarrow -it$, the gauge fields (31) describe a spherically outgoing (incoming) luminal thin shell, as the exiting sphaleron explodes (implodes) on its way downhill (uphill). The luminal shell supports only light-like fields which are purely transverse, and fall off as $1/t$ at large times. It was previously used to describe ‘‘sphaleron explosion’’ in [24].

The fixed energy topological solutions contribute to Wilson lines, as a heavy quark travels from one vacuum to another vacuum with one added (sub-

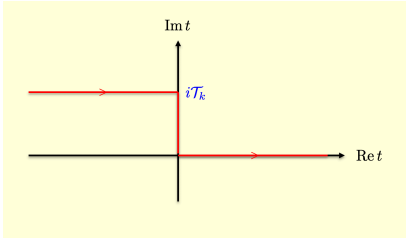


FIG. 8. Zig-zag path for a temporal Wilson line describing a heavy-quark traveling from one vacuum to another with a different topological charge, and riding a fixed energy tunneling configuration with tunneling time \mathcal{T}_k .

tracted) topological charge. In Minkowski signature, it corresponds to the zig-zag path shown in Fig. 8,

$$\mathcal{C} =] - \infty + i\mathcal{T}_k, i\mathcal{T}_k] \cup [i\mathcal{T}_k, 0] \cup [0, +\infty[\quad (35)$$

where on the purely imaginary $[i\mathcal{T}_k, 0]$ path, the heavy quark is riding the tunneling process. A similar path choice was also advocated for scattering processes through instantons in [49].

The chief contribution to the time-like Wilson line follows from this path, since the gauge field on the paths with real time support is luminal and transverse asymptotically,

$$W(r; k) = \exp \left(i \left[\int_{-\infty + i\mathcal{T}_k}^{i\mathcal{T}_k} dt \frac{1}{2} A_4^a(-it, r; k) \tau^a + \int_{i\mathcal{T}_k}^0 dt \frac{1}{2} A_4^a(-it, r; k) \tau^a + \int_0^{\infty} dt \frac{1}{2} A_4^a(-it, r; k) \tau^a \right] \right) \quad (36)$$

At the sphaleron point with $f_{k=0} = 1/2$, we can check that $W(r; k = 0) = 1$ and no self-energy is generated in going through a finite energy tunneling configuration. This result follows by deforming the contour on the real axis, without encountering poles for $\mathcal{T}_{k=0} < \rho$, and noting that A_4 is time-odd. Away from the sphaleron point, a fraction of the instanton self-energy can be picked, through the emergence of complex singularities solution to $f_k(\xi) = \infty$.

III. SPIN-DEPENDENT POTENTIALS

A. Phenomenology, from heavy to light quarks

To start, let us consider the first $1S$ -shell, with zero orbital momentum $L = 0$, to recall the magnitude of the spin-spin forces. Starting from heavy quarkonia and proceeding to lighter systems, we focus on the following selection of mass splittings (all in MeV)

$$M(\Upsilon) - M(\eta_b) = 61.; \quad (37)$$

$$M(J/\psi) - M(\eta_c) = 116.; \quad M(\psi^{2S}) - M(\eta_c^{2S}) = 51.$$

$$M(B^*) - M(B) = 35.5; \quad M(D^*) - M(D) = 137.$$

$$M(K^*) - M(K) = 398.; \quad M(\rho) - M(\pi) = 636.$$

Note that these splittings grow for lighter quarks, eventually getting comparable to the scale of the mesonic masses: therefore in those case spin forces cannot be treated as a perturbation.

Naively, the flavor dependence of the spin-spin forces should just follow from the product of the quark magnetic moments, which is $\sim 1/m_{Q_1}m_{Q_2}$, times some universal magnetic fields in the QCD vacuum as defined in the correlators of section B. Yet the select splittings above show that it is not the case even for heavy quarks: e.g. charm and bottom effects are different by a factor of two, not 10 as the mass ratio would suggest. Yet universal vacuum correlators /potentials do not imply universal (mass-independent) matrix elements, since all these mesons have vastly different wave functions. Especially interesting is the case of charmonium (second line in (37)) in which one has both the splittings of $1S$ and $2S$ levels. Not only the overall volume and $\psi(r=0)$ are different, but also the wave function of $2S$ state has a node. The ratio of wave functions squared is shown in Fig.9, and one can see that it changes from 0.538 at $r = 0$ to zero at $r \approx 2 GeV^{-1}$. The ratio of the observed splittings is $51./113. \approx 0.45$ is comfortably in between, but much closer to the former number than to the latter one. This observation alone tells us that V_{SS} must be concentrated at very

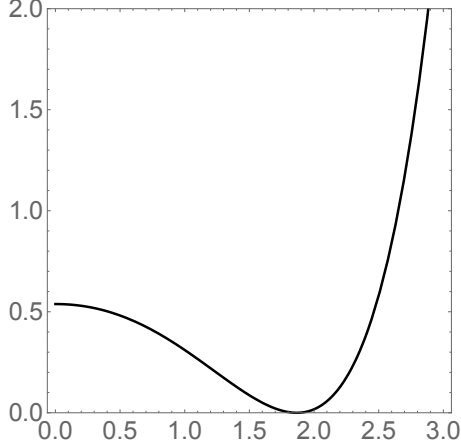


FIG. 9. The ratio of wave functions squared $\psi_{2S}(r)^2/\psi_{1S}(r)^2$ as a function of distance $r(\text{GeV}^{-1})$.

small distances.

Going further in phenomenology, we now proceed to the 1-P shell, with $L = 1$. For any flavor combination, there are 4 states we will be interested in as above, starting from heavy quarkonia, to heavy-light and all the way to mesons made of light quarks. For the light mesons we select two channels, the strange-light K mesons and charge $I = 1$ sector of the light-light. (The $I = 0$ sector has complicated mixing between quark states and glueballs, which we prefer not to include.) The results are listed in Table I. For example, the χ_{b2} state is the $\bar{b}b$ state with $S = 1, L = 1, J = 2$, and the h_b state has $S = 0, L = 1, J = 1$. All the names and masses are from the 2020 PDG tables

With $L = 1$ all the three spin-dependent terms come into play, and with four masses one has three differences which allow us to solve for each individual contribution. We define the differences from the χ to h states as

$$a\langle(\vec{S} \cdot \vec{L})\rangle + b\langle S_{12}\rangle + c\langle(\vec{S}_1 \cdot \vec{S}_2)\rangle$$

We can solve for a, b, c by using the corresponding

quantum numbers for these states, namely

$$\begin{aligned} M(\chi_{b2}) - M(h_b) &= a - (2/5)b + c, \\ M(\chi_{b1}) - M(h_b) &= -a + 2b + c, \\ M(\chi_{b0}) - M(h_b) &= -2a - 4b + c \end{aligned} \quad (38)$$

The results are listed in the last three columns of Table I. The ensuing comments are:

- (i) The *spin-orbit* matrix element a for heavy quarks, is dominant;
- (ii) The *spin-orbit* gets smaller for light quarks. Why?
- (iii) The *tensor force* grows for heavy-light but then flips sign for light quarks. Why?
- (iv) The *spin-spin* term grows and is dominant for light quarks.

We now proceed to see whether these observations can be explained by the theory we discuss below.

B. Wilson lines and the five potentials

Eichten and Feinberg [7] defined general spin-dependent interactions of heavy quarks in terms of a priori five potentials (see their definitions and further discussion in appendix A) which contribute as follows

TABLE I. The first column is the flavor composition. The next four columns refer to four states of the $n = 1, P$ -shell with the quantum numbers explained in the text. The last three columns are matrix elements of spin-orbit, tensor and spin-spin terms, in MeV.

	S=1, J=2	S=1, J=1	S=1, J=0	S=0, J=1	a	b	c
$\bar{b}b$	$\chi_{b2}(9912)$	$\chi_{b1}(9893)$	$\chi_{b0}(9859)$	$h_b(9899)$	13.7	3.3	0.5
$\bar{c}c$	$\chi_{c2}(3556)$	$\chi_{c1}(3511)$	$\chi_{c0}(3415)$	$h_c(3525)$	35.	10.	0.1
$\bar{c}q$	$D_2^*(2461)$	$D_1(2430)$	$D_0^*(2300)$	$D_1(2421)$	34.	16.	12.
$\bar{s}q$	$K_2(1430)$	$K_1(1403)$	$K_0(1430)$	$h_s(1270)$	6.7	-5.6	151.
$\bar{q}q$	$a_2(1317)$	$a_1(1230)$	$a_0(1450)$	$b_1(1235)$	0.5	-36.	68.

$$\begin{aligned} V_{SD} &= \left(\frac{S_Q \cdot L_Q}{2m_Q^2} - \frac{S_{\bar{Q}} \cdot L_{\bar{Q}}}{2m_{\bar{Q}}^2} \right) \left(\frac{1}{r} \frac{d}{dr} (V_C(r) + 2V_1(r)) \right) \\ &+ \left(\frac{S_{\bar{Q}} \cdot L_Q}{m_Q m_{\bar{Q}}} - \frac{S_Q \cdot L_{\bar{Q}}}{m_{\bar{Q}} m_Q} \right) \left(\frac{1}{r} \frac{d}{dr} V_2(r) \right) + \frac{(3S_Q \cdot \hat{r} S_{\bar{Q}} \cdot \hat{r} - S_Q \cdot S_{\bar{Q}})}{3m_Q m_{\bar{Q}}} V_3(r) + \frac{1}{3} \frac{S_Q \cdot S_{\bar{Q}}}{m_Q m_{\bar{Q}}} V_4(r) \end{aligned} \quad (39)$$

$\vec{S}_{Q,\bar{Q}}$ and $\vec{L}_{Q,\bar{Q}}$ are the spin and orbital angular momenta of the $\bar{Q}Q$ pair. $V(r)$ is the central static potential, $V_1(r)$ and $V_2(r)$ are obtained by inserting a chromo-electric or chromo-magnetic field on the temporal Wilson loop. The spin-spin and tensor contributions $V_{3,4}(r)$ follow from the insertion of two chromo-magnetic fields on the Wilson loop. (39) is exact to order $1/m_Q^2$. The last spin-spin part is fixed as $V_4(r) = 2\nabla^2 V_2(r)$ [7]. Lorentz invariance ties the central potential $V_C(r)$ to the spin-orbit potentials $V_{1,2}(r)$ through the so called Gromes relation [50]

$$V_C(r) = V_2(r) - V_1(r) \quad (40)$$

The spin-dependent contributions emerging from the string were discussed by Buchmuller [51] and others [50, 52]. Since the spin-spin interactions are short ranged, only the spin-orbit contributions survive at large separation b_\perp . This is manifest from (40) with $V_2(r) \rightarrow 0$ and $V_C(r) \rightarrow -V_1(r)$ asymptotically, hence [50–52]

$$\begin{aligned} V_{SL,\text{string}}(b_\perp) &= -\left(\frac{S_Q \cdot L_Q}{2m_Q^2} - \frac{S_{\bar{Q}} \cdot L_{\bar{Q}}}{2m_{\bar{Q}}^2}\right) \frac{\sigma_T}{b_\perp} \\ &\rightarrow -\frac{\sigma_T}{2m_Q^2 b_\perp} S \cdot L \end{aligned} \quad (41)$$

with $V_C(r) = \sigma_T r$, $\vec{S} = \vec{S}_Q + \vec{S}_{\bar{Q}}$ and $\vec{L} = \vec{L}_Q = -\vec{L}_{\bar{Q}}$. Since the electric flux tube is confined to the string, the spin-orbit contribution is only due to Thomas precession which is of opposite sign and half the spin-orbit contribution from the central potential. This can be understood from (39–40) if we assume that $V_2(r)$ is short range, so that $V_C(r) = -V_1(r)$. This string-induced spin-orbit effect is dubbed scalar-like in contrast to the Coulomb-induced spin-orbit effect which is vector-like.

C. Lattice studies

The static spin-spin potentials have been evaluated on the lattice, using correlators of Wilson lines with explicit field strengths. In particular, Koma and Koma [53] find that while V_{SS} is indeed rather short range, it does not fit to the vector+scalar exchange paradigm: a pseudo-scalar glueball exchange has been proposed. Skipping a decade, Kawanai and Sasaki [54] accurately derived the central and spin-spin potentials for the $\bar{c}c$ and $\bar{s}s$ families, and used

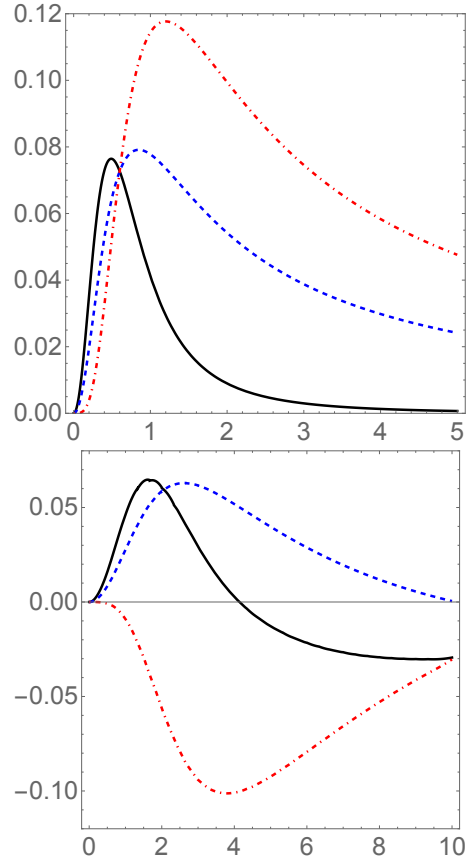


FIG. 10. Perturbative (upper plot) and instanton-induced (lower plot) spin-dependent potentials for charmonium. The black solid, blue dashed and red dash-dotted lines are for $r^2 V_{SS}, r^2 V_{SL}, r^2 V_T$, in GeV^{-1} , versus r in GeV^{-1} .

them in effective Schrodinger equations for a spectroscopic analysis with nice agreement with the spectroscopic data. In Fig. 13 we show (solid line) their exponential fit (for $\bar{c}c$).

$$V_{SS}^{\bar{c}c} \equiv \alpha e^{-\beta r}, \quad \alpha = 2.15 \text{ GeV}, \quad \beta = 2.93 \text{ GeV} \quad (42)$$

Let us try to interpret this result: Naively, the coefficient in the exponent should be the mass of the object exchanged: for a gluon it should be about half of glueball masses, of the order of 1 GeV or so. It is in fact larger by a factor of 3. Why is it so large?

Fortunately, one can check it phenomenologically and find that it does describe well the $2S$ to $1S$ splitting in charmonium. Using this V_{SS} parameterization from [54] we calculate $1S$ triplet-singlet splitting to be 113.7 MeV (exp: 113 MeV) and $2S$ to be 47.3 MeV (exp: 51 MeV). While not perfect,

this version of V_{SS} clearly does the job, at least in charmonium.

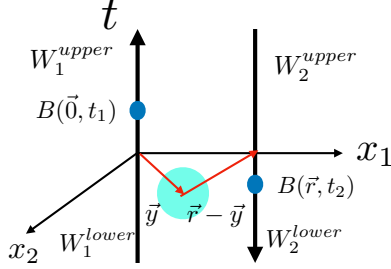


FIG. 11. Notations of vectors in evaluation of Wilson lines with two field strengths.

D. Spin-dependent forces from instantons

We decided first not to rely on general relations, sometimes leading to singular functions, and evaluated the correlators of Wilson lines with fields directly.

The notations we use for the evaluation of the spin-dependent potentials are shown in Fig. 11. The Wilson line W_1 is located at the origin of the spatial coordinates $\vec{0}$, and W_2 at $\vec{r} = (r, 0, 0)$. Two magnetic fields are inserted on them, and act at times t_1 and t_2 , respectively. The SU(2) color matrix associated with the field B_m is τ^m , and the overall color trace defines the following tensor

$$C^{m\bar{m}} = \text{Tr} [W_1^{\text{upper}} (W_2^{\text{upper}})^{+\tau^{\bar{m}}} (W_2^{\text{lower}})^{+\tau^m} W_1^{\text{lower}} \tau^m]$$

This construction is implicitly included in what we denote by the “double average”, for example the spin-spin potential is related to correlator of two magnetic fields integrated over their time difference

$$V_4(r) = \int dt \langle \langle B^{ma}(\vec{0}, 0) B^{ma}(\vec{r}, t) \rangle \rangle \quad (43)$$

$$\begin{aligned} A_1^{\text{lower}} &= -\left[\pi + 2 \arctan\left(\frac{t_1}{\sqrt{y^2 + \rho^2}}\right) \right] \frac{1}{\sqrt{1 + \rho^2/y^2}} \\ A_2^{\text{lower}} &= -\left[\pi + 2 \arctan\left(\frac{t_2}{\sqrt{r^2 + y^2 - 2ry\cos(\theta) + \rho^2}}\right) \right] \frac{1}{\sqrt{1 + \rho^2/(r^2 + y^2 - 2ry\cos(\theta))}} \end{aligned} \quad (45)$$

The “upper” lines are given by the same expressions

The center of the instanton is put at time zero and spatial location \vec{y} . On dimensional grounds, the instanton of size ρ should contribute to those potentials $\sim \kappa 1/\rho^3 F(r/\rho)$.

The field strength for an instanton (in regular gauge), located at point y , is

$$G_{\mu\nu}^a(x) = -4\eta_{\mu\nu}^a \frac{\rho^2}{((x-y)^2 + \rho^2)^2} \quad (44)$$

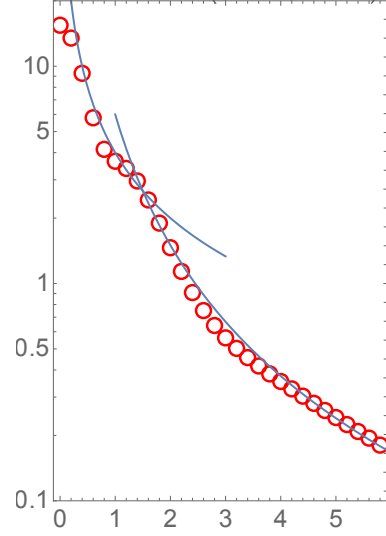


FIG. 12. The dependence of the integrated correlator of two magnetic fields (43) on the distance, in units of r/ρ , is shown by points. The two thin lines are drawn for comparison, the upper is $\sim 1/r$ and the lower $\sim 1/r^2$.

Four Wilson lines are written in their canonical form $W = \cos(A) + i(\vec{n}\vec{\tau})\sin(A)$ with certain angles, which in regular gauge are

with opposite signs of arctan. If there is no field

insertions, these terms cancel as they should, and their sum become the angles we already met in the expression for central potentials.

In total, the correlator includes integration over d^3y, t_1, t_2 . With the azimuthal angle ϕ_y being irrelevant, it is 4-dimensional integral performed numerically. The results are shown in Fig.12. In this log plot one can see that the resulting spin-spin force rapidly decreases with distance. For comparison, we show two lines with $1/r$ and $1/r^2$, which ap-

proximately reproduces the behavior. One should not however conclude that they give correct analytic asymptotic: in fact, expanding the integrand in inverse powers of r leads to divergences of the remaining integrals, indicating that the true asymptotic behavior cannot be just powers.

In the instanton vacuum, with (anti) selfdual fields $\vec{E}^a = \pm \vec{B}^a$ in Euclidean signature, all potentials in (39) can be tied to the central potential $V_C(r)$ [6, 7, 43]

$$V_C(r) + 2V_1(r) \rightarrow 0 \quad V_2(r) \rightarrow \frac{1}{2}V_C(r) \quad V_3(r) \rightarrow -\left(\frac{1}{r}V'_C - V''_C\right) \quad (46)$$

and the simplified spin-orbit contribution

$$\left[\frac{1}{2m_Q^2} \frac{1}{r} \frac{d}{dr} V_C(r)\right] (S_Q + S_{\bar{Q}}) \cdot L_Q \equiv \left[\frac{1}{2m_Q^2} \frac{1}{r} \frac{d}{dr} V_C(r)\right] S \cdot L \quad (47)$$

Schematically, the central electric interaction $\langle E_i^a(x)[x, 0]^{ab} E_i^b(0) \rangle$ is amenable to the spin-orbit interaction $\langle E_i^a(x)[x, 0]^{ab} B_i^b(0) \rangle$ and also the spin-spin and tensor interaction $\langle B_i^a(x)[x, 0]^{ab} B_i^b(0) \rangle$.

In Fig.13 we compare the perturbative (dashed-

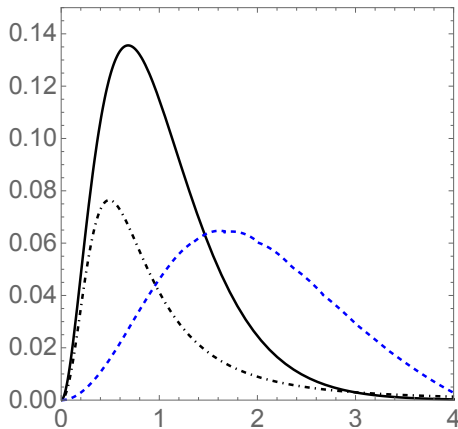


FIG. 13. Spin-spin potential for $\bar{c}c$ system multiplied by distance squared $r^2 V_{SS} (GeV^{-1})$ versus $r (GeV)^{-1}$. The solid line is the exponential fit (42) to lattice measurements [54]. The dash-dotted line shows the regulated laplacian of the Coulomb potential (48) with $\delta = 0.6 GeV^{-1}$. The blue dashed line show the instanton contribution. Note that the area under the last two curves is roughly equal to that under solid one, the lattice fit.

dotted-black) and nonperturbative (dashed-blue) spin-spin potentials with the lattice result (solid-black). Recall that the Laplacian of the Coulomb force is a delta function, well known in atomic and positronium physics. However, one should use Coulomb potential $1/r$ in some regulated form, for several reasons. First, when the potential gets as deep as (minus) mass, the nonrelativistic approximation itself should break down, so the spread cannot be smaller than $O(1/m_Q)$. Second, lattice studies include non-locality in the form of the lattice spacing a . Third, a Gaussian-smeared delta function is actually used in many spectroscopic calculations, see e.g. [56]. For the perturbative spin-spin interaction, we use a simpler version, as the Laplacian of a Coulomb contribution regulated by a fixed parameter $\delta = 0.6 GeV^{-1}$

$$V_{SS}^C(r) = -\frac{A}{3m_Q m_{\bar{Q}}} \vec{\nabla}^2 \frac{1}{\sqrt{r^2 + \delta^2}} \quad (48)$$

For the nonperturbative spin-spin part, we use the instanton contribution, which is given by the Laplacian acting on the central potential

$$V_{SS}^{inst}(r) = \frac{1}{3m_Q m_{\bar{Q}}} \vec{\nabla}^2 V_C^{inst}(r) \quad (49)$$

All the potentials shown are multiplied by r^2 , as they appear in the volume integrals. So, if the wave functions are roughly constant at this small scale, the area under the curves in Fig. 13 gives an estimate

TABLE II. “Hyperfine” splittings of certain $L = 0$ mesons with $J = 1$ and $J = 0$. The first row of numbers shows the experimental values (MeV) (rounded to 1 MeV). The second row gives the matrix elements of the lattice-based spin-spin potential (42), the next two rows are the (regulated) Coulomb and instanton-induced spin-spin contributions.

flavors	$M_{\Upsilon} - M_{\eta_b}$	$M_{J/\psi} - M_{\eta_c}$	$M(D^*) - M(D)$	$M(K^*) - M(K)$	$M(\rho) - M(\pi)$
Exp	61.	116.	137.	398.	636.
$\langle V_{SS}^{\text{lat}}/3m_Q m_{\bar{Q}} \rangle$	46.	108.	98.	170.	
$\langle \vec{\nabla}^2 V_C/3m_Q m_{\bar{Q}} \rangle$	28.	58.	48.	82.	
$\langle \vec{\nabla}^2 V_{\text{inst}}/3m_Q m_{\bar{Q}} \rangle$	7.	30.	48.	90.	

of the relative contributions. So, one finds that the perturbative and non-perturbative parts contribute *comparably* to the total spin-spin potential, in sum roughly reproducing the lattice-based result. This observation is among the main findings of this work.

Of course, the actual magnitude of the spin splittings depends on the quark masses involved, explicitly via $1/m_Q^2$ factors and implicitly, via the wave functions. Lighter quarks lead generally to hadrons of larger size, or smaller wave functions at small distances.

The matrix elements of all three potentials shown in Fig. 13 were evaluated using wavefunctions from the Cornell potential irrespective of flavor. The results for the spin-spin contributions are in Table II. The results show that perturbative and non-perturbative contributions for heavy quarkonia do reproduce the splittings if *taken together*. Already for heavy-light mesons one can see that some additional effect seems to be missing: it will indeed so as will be explained below. Furthermore, for the mesons containing only light quarks both contribu-

tions together definitely fail to describe large splittings seen experimentally. Clearly some other effects are in play here, to be discussed below.

We continue our phenomenological description of the spin-dependent interactions, by considering the next four states in the 1P shell, with the onset of the spin-orbit and tensor potentials. The empirical information to be used on several mesonic families is listed in III. The theoretical estimates follow from 1P wave functions derived with standard Cornell potential. For both components of the central potential – perturbative and instanton-induced – we calculated the matrix elements of the three spin-dependent potentials using the formulae given above, and then calculated their matrix elements in the 1P shell.

One observation from this table is that the “theory” (the sum of the last two rows) and the lattice-induced one (the second row) are basically in agreement. The other is that their disagreement with experiment (the upper row) is dramatically growing for light quark systems. This implies that for light quarks something important is missed, in the description as developed so far.

E. Contributions of $I\bar{I}$ molecules to spin forces

Like in subsection II B, let us start with the $I\bar{I}$ molecules oriented in the time direction, for which $\vec{E} \sim G_{4m}$ and A_4 are time-odd. Therefore, as we noted before, there is no contribution to the central potential.

Yet the *spin-spin and tensor* forces are not at all zero, as the main contributors to the correlator come

from the *magnetic* fields \vec{B} , which have *the same sign* in the I and \bar{I} parts of the molecule!

A detailed description of the $I\bar{I}$ configuration can be achieved by the Yung ansatz, which is quite accurate. The corresponding expressions for field strengths were obtained in Mathematica, which are way too complicated to be given here. Yet the field strengths are approximately additive, and this approximation will be used in what follows.

TABLE III. Groups of three matrix elements of spin-spin, spin-orbit and tensor potentials V_{SS}, V_{SL}, V_T , respectively. The first one in each group is the observed “exp” value from Table I, the second and the third values are the perturbative and instanton-induced contributions, corresponding to the Coulomb and instanton-induced parts of the central potential.

	SS “exp”	SS pert	SS inst	SL “exp”	SL pert	SL inst	T “exp”	T pert	T inst
$\bar{c}c$	0.1	0.56	1.9	35.	3.2	3.8	10.	5.8	-5.7
$\bar{s}q$	151.	5.	29.	6.7	31.	38.	-5.6	58.	-46.
$\bar{q}q$	68.	8.	48.	0.5	52.	64.	-36.	96.	-78.

Let us start with the correlator of two magnetic

fields, measured at integrated times t_1 and t_2 on two temporal lines separated by a spatial distance r

$$\int dt \langle B^{ma}(0, \vec{0}) B^{ma}(t, \vec{0}) \rangle = \int dt_1 dt_2 d^3y (48n_{mol}\rho^4) \times \left(\frac{1}{((t_1 - R/2)^2 + \rho^2 + y^2)^2} + \frac{1}{((t_1 + R/2)^2 + \rho^2 + y^2)^2} \right) \times \left(\frac{1}{((t_2 - R/2)^2 + \rho^2 + y_2^2)^2} + \frac{1}{((t_2 + R/2)^2 + \rho^2 + y_2^2)^2} \right) \quad (50)$$

Here y^2 and $y_2^2 = y^2 + r^2 - 2ry\cos(\theta_{ry})$ are the squared 3d distances to the first and second Wilson lines. We assumed additivity of the magnetic fields from I and \bar{I} , and ignored the color rotation angles on the Wilson lines (which vanish at the instanton center, as we already know).

At zero distance between the line $r = 0$, all integrations can be done analytically, with the result

$$\int dt \langle B_1^{ma}(0, \vec{0}) B_2^{ma}(t, \vec{0}) \rangle_{r=0} = 12\pi^4 \rho n_{mol} \quad (51)$$

For qualitative orientation, one can compare this ex-

pression to (the extrapolation of) the lattice spin-spin potential (42) to $r = 0$: they are equal if $n_{mol} \approx 7 fm^{-4}$.

Note that in this approximation there is no dependence on the (time) separation R of I and \bar{I} centers. For nonzero r the volume integral over $y, \cos(\theta_{ry})$ is done numerically, see the results in Fig. 14.

Now let us calculate the same correlator, but for a molecule rotated so that its vector R_μ joining the centers, lines in the spatial direction, say the same as the vector \vec{r} between the Wilson lines. The electric and certain magnetic fields exchange places and the expression changes into

$$\int dt \langle B^{am}(0, \vec{0}) \vec{B}^{am}(t, \vec{0}) \rangle = \int dt_1 dt_2 dy_1 2\pi y_\perp dy_\perp (48n_{mol}\rho^4) \times \left(\frac{1}{(t_1^2 + \rho^2 + (y_1 - R/2)^2 + y_\perp^2)^2} - \frac{1}{(t_1^2 + (y_1 + R/2)^2 + \rho^2 + y_\perp^2)^2} \right) \times \left(\frac{1}{(t_2^2 + \rho^2 + (y_1 - R/2 + r)^2 + y_\perp^2)^2} - \frac{1}{(t_2^2 + (y_1 + R/2 + r)^2 + \rho^2 + y_\perp^2)^2} \right) \quad (52)$$

In Fig. 14 we compare the correlators for two molecule orientations with averaging factors,

(1/4)(50) and (3/4)(52) by upper and lower points, as well as their sum (the line). So, while the two contributions have different dependence on r , the orientation-average $V_{SS}(r)$ decreases monotonously, and has the effective width (at half maximum) close to the average instanton size ρ . Note that this range is shorter than $V_{SS}(r)$ from the instantons alone (calculated from the Laplacian of the contribution to the central potential in the previous subsection), and it does not have a negative part. It is therefore closer in shape to what was found on the lattice.

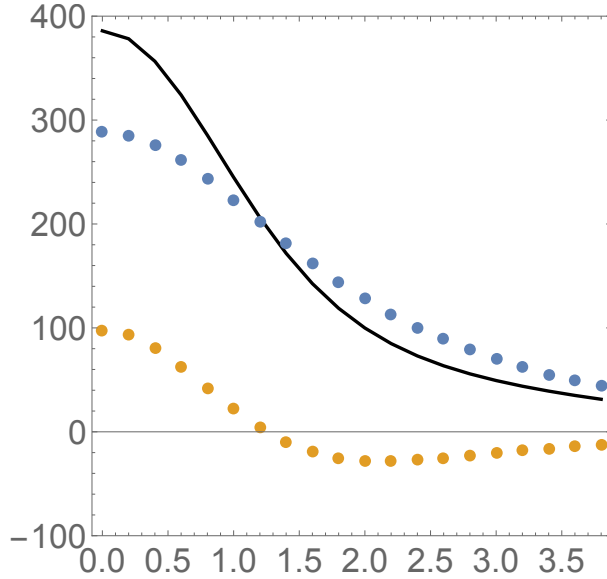


FIG. 14. The normalized correlators (1/4)(50) (upper points) and (3/4)(52) for $R = \rho$ (lower points) in units of $n_{mol}\rho$, versus the distance between the Wilson lines r/ρ . The solid line shows their sum.

The *spin-orbit* force is qualitatively different from spin-spin ones, being related to a correlator $\int dt \vec{E} \vec{B}$.

For a time-oriented molecule $R_\mu = (0, 0, 0, R)$ $\vec{E}(t)$ is time-odd and $\vec{B}(t)$ is time-even, so for this molecule orientation this correlator vanishes. The situation is different for a space-oriented molecule, say along x_1 . Now G_{1m} , $m = 2, 3, 4$ fields are odd in x_1 inversion, but everything is even along the time axes. The expression for the correlator can easily be constructed and calculated in a way similar to what was done above for $V_{SS}(r)$

We conclude that the “molecule-induced” spin forces are quite similar to the instanton induced ones (apart of course normalization to quite different densities) at small distances, but are *significantly reduced* at $r > 2\rho$ due to the partial cancellations by different orientations.

In the previous section we have seen that, in the approximation of molecules represented as two independent pseudoparticles, the non-perturbative $V_{SS}(r)$ have about the right magnitude, but somewhat too large range. We now see that a better description of the field structure has the potential to remedy this problem.

F. Contributions of the fixed energy tunneling configurations to spin forces

The finite energy tunneling configurations contribute to the spin forces, through close Wilson loops dressed by E, B fields. However, since these configurations cease to be self-dual for $0 \leq k < 1$, the induced spin potentials are in general independent. Moreover, these configurations carry t-odd electric fields, and are purely magnetic at the exit points ($t_E = 0$). They may only contribute to the spin-spin and tensor potentials.

The explicit expression of the magnetic field in Euclidean time is

$$\begin{aligned}
 B^{ma}(t_E, \vec{x}) = & \delta^{ma} \left(-\frac{16\rho^2}{\mathbb{D}} f + \frac{8\rho^2 r^2}{\mathbb{D}^2} fF + \frac{32\rho^3 t_E r^2}{\mathbb{D}^2} f' + \frac{32r^2 \rho^2}{\mathbb{D}^2} f^2 \bar{F} \right) \\
 & + x^m x^a \left(-\frac{8\rho^2}{\mathbb{D}^2} fF - \frac{32t_E \rho^3}{\mathbb{D}^2} f' + \frac{32\rho^2}{\mathbb{D}^2} f^2 F \right) \\
 & + \epsilon^{mai} x^i \left(\frac{16\rho}{\mathbb{D}} f + \frac{4\rho}{\mathbb{D}^2} fF\bar{F} + \frac{16t_E \rho^2}{\mathbb{D}^2} f' \bar{F} - \frac{32\rho^3}{\mathbb{D}^2} (2r^2 + \bar{F}) f^2 \right)
 \end{aligned} \quad (53)$$

with $f' = \partial_\xi f_k(\xi)$,

$$\mathbb{D} = (t_E^2 + r^2 + \rho^2)^2 - 4t_E^2 \rho^2 \quad (54)$$

and

$$F = t_E^2 + r^2 + \rho^2 \quad \bar{F} = -t_E^2 - r^2 + \rho^2 \quad (55)$$

The magnetic field in Minkowski signature follows from the substitution $t_E \rightarrow -it$.

The induced spin-spin interaction follows from the

$$\int_{\mathcal{C}} dt \int_{\bar{\mathcal{C}}} d\bar{t} \langle B^{ma}(-it, \vec{0}) B^{ma}(-i\bar{t}, \vec{0}) \rangle = [3 \cdot 2^8 \rho^4 n_k] \int_{\mathcal{C}} dt \int_{\bar{\mathcal{C}}} d\bar{t} \int d^4 Z \left(\frac{f \bar{f}}{\mathbb{D} \bar{\mathbb{D}}} \right) \quad (56)$$

with now

$$\begin{aligned} \mathbb{D} &\rightarrow ((-it - Z_4)^2 + \vec{Z}^2 + \rho^2)^2 - 4(-it - Z_4)^2 \rho^2 \\ \bar{\mathbb{D}} &\rightarrow ((-i\bar{t} - Z_4)^2 + \vec{Z}^2 + \rho^2)^2 - 4(-i\bar{t} - Z_4)^2 \rho^2 \end{aligned} \quad (57)$$

and $F = f_k(\xi)$ and $\bar{f} = f_k(\bar{\xi})$ with

$$\begin{aligned} \xi &\rightarrow \frac{1}{2} \ln \left(\frac{(-it - Z_4 + \rho)^2 + \vec{Z}^2}{(-it - Z_4 - \rho)^2 + \vec{Z}^2} \right) \\ \bar{\xi} &\rightarrow \frac{1}{2} \ln \left(\frac{(-i\bar{t} - Z_4 + \rho)^2 + \vec{Z}^2}{(-i\bar{t} - Z_4 - \rho)^2 + \vec{Z}^2} \right) \end{aligned} \quad (58)$$

with the Euclidean-Minkowski time assignments in (35).

At the sphaleron point $f_{k=0} = 1/2$, and (56) reduces to

$$\begin{aligned} \int_{\mathcal{C}} dt \int_{\bar{\mathcal{C}}} d\bar{t} \langle B^{ma}(-it, \vec{0}) B^{ma}(-i\bar{t}, \vec{0}) \rangle &\rightarrow [192 \rho^4 n_{k=0}] \int_{\mathcal{C}} dt \int_{\bar{\mathcal{C}}} d\bar{t} \int d^4 Z \\ &\times \frac{1}{(((-it - Z_4)^2 + \vec{Z}^2 + \rho^2)^2 - 4(-it - Z_4)^2 \rho^2) (((-i\bar{t} - Z_4)^2 + \vec{Z}^2 + \rho^2)^2 - 4(-i\bar{t} - Z_4)^2 \rho^2)} \end{aligned} \quad (59)$$

Overall time translational invariance allows us to set $Z_4 = 0$ in the integrand, with the final result

$$\frac{\int_{\mathcal{C}} dt \int_{\bar{\mathcal{C}}} d\bar{t} \langle B^{ma}(t, \vec{0}) B^{ma}(\bar{t}, \vec{0}) \rangle}{\int dZ_4} = \frac{\pi^4}{4\rho^3} \quad (60)$$

This result follows by deforming the complexified path to the real axis, without encountering poles for $\mathcal{T}_{k=0} < \rho$. The spin-spin interaction (60) stemming from the finite energy tunneling configurations, is comparable to the spin-spin interaction (51) from the thimbles. At the sphaleron point and for zero separation, they are comparable when

$$\frac{n_{k=0}}{n_{\text{mol}}} = \frac{12\pi^4}{192\pi^4/4} = \frac{1}{4} \quad (61)$$

complexified path in the t-plane shown in Fig. 8. An estimate of the magnitude of the spin-spin interaction, follows from zero separation between a path \mathcal{C} and $\bar{\mathcal{C}}$

IV. INTERQUARK FORCES INDUCED BY INSTANTON ZERO MODES ('T HOOFT EFFECTIVE LAGRANGIAN)

A. Pseudoscalar mesons which are and are not the Nambu-Goldstone modes

It is known since 1970's that in the chiral limit light-quark pseudoscalar mesons consist of octet π, K, η Nambu-Goldstone modes and a singlet η' which does *not* belong to that set, and is instead very heavy. It happens because the t' Hooft effective Lagrangian violates $U_A(1)$ and quite effectively

generates flavor-changing annihilation processes

$$\bar{u}u \leftrightarrow \bar{d}d \leftrightarrow \bar{s}s$$

When a strange quark mass is added, one finds $\eta-\eta'$ mixing which describes well the phenomenology of their decays. It sharply contrasts with the vector counterparts, ρ, ω, ϕ mesons, for which the mixing is very small.

To avoid these annihilation processes, one can discuss “flavored” channels, like $\pi^+ = \bar{d}u$, in which case the t’ Hooft effective Lagrangian acts as a force between the quark and antiquark. Yet it is still different from the conventional forces we so far discussed, in that it exists for quarks of *different flavors* only. In Fig.1 we illustrate how the t’ Hooft induced vertex operates in the pion and rho charged meson channels.

Before we turn to specifics, let us comment on some lattice implementations of theories with different quarks. The simplest case is a single quark flavor theory, $N_f = 1$. In it the t’ Hooft action is a 2-fermion operator: it gives the quark an effective mass, but does not generate annihilations or interactions as we noted. The only pseudoscalar mesons is the analog of η' , no π, K, η modes exist.

In lattice implementations nowadays one uses gauge ensemble for physical QCD, but still use certain diagram and mass selections aiming to study certain unphysical particles. For example, in [57], an artificial particle called η_s made of $\bar{s}s$ was introduced, with no mixing to other flavors. Its properties are deduced from the *connected* diagram, without the disconnected one in which the flavor is changed. One may explain its absence by introducing an *extra* valence quark species s' , and view source/sink operators as flavor-nondiagonal $\bar{s}s'$. Our comment is that such setting, while eliminating the annihilations, still keeps the t’ Hooft effective Lagrangian producing a force between the quark and antiquark, as they are not of the same flavor. Apart from the mass values, this channel is no different from say $\pi^+ = \bar{d}u$ we consider.

In our first take on spin-spin forces in (37) we already observed anomalously large splitting between the $\rho, S = 1$ and $\pi, S = 0$ states in the lowest light quark shell, and have seen that the magnitude of $V_{SS}(r)$ discussed so far, is not sufficient to explain it.

(In particular, adding $V_{SS}(r)$ as detailed above to the basic quark model, with the Cornell potential and a light quark constituent mass of 0.35 GeV, re-

duces the ground state 1S mass substantially, from 1.4 GeV to about 0.85 GeV. Yet it is still far from the observed pion mass of 0.138 GeV and from zero, which it should be in the chiral limit.) Of course, a correct pion mass can only be explained in an approach, consistently explaining chiral symmetry breaking, as well as other parameters of chiral perturbation theory. Two famous models – NJL and ILM – are well known examples of that.

Before we focus on the theory, let us return for a brief moment to the phenomenological constituent quark model, to see what kind of interaction one needs to add in order to obtain the experimentally observed pions. Let us assume that there is an additional interaction, that operates *only* between quarks of different flavors, on top of the flavor-blind forces so far discussed. Note that the usual discussion of $\pi-\eta'$ splitting is based on “annihilation channels” (like $\bar{u}u \leftrightarrow \bar{d}d$) as we continue to consider only charged mesons, like $\bar{d}u$.

The t’ Hooft Lagrangian is usually written as a local operator *a la* NJL one, corresponding to a potential of the type $G_{\text{Hooft}}\delta^3(\vec{r})$ potential. This form assumes that the instanton size ρ is much smaller than the hadronic sizes, as it appears in the standard LSZ “amputation” of external propagator lines. Unfortunately, in the Euclidean setting of the instanton calculus, taking these lines on-shell amounts to the limit $p^\mu \rightarrow 0$ for all components. And yet, it is clear that the process is nonlocal, and that the scale of its size is ρ . Thus in model applications one include form-factors, usually the Fourier transform of the zero modes. We will use another “regulated delta function” form described in section C.

(Comment: When the nonlocality induced by the parameter ρ is small compared to the hadron size, it can be well approximated by a delta function. However, this is not true for pions. This can be seen from the pion wave function (with or without the effective t’ Hooft term): its $r^2\psi_\pi^2(r)$ peaks at $r \approx \rho$. In this case. Therefore, in the pion case there a remains certain dependence on a choice of the non-local approximation.)

Finally, the coupling strength for the t’ Hooft effective interaction to add to the discussed potentials above needed to reproduce the physical pion mass is found to be

$$G_{\text{Hooft}} = 17 \text{ GeV}^{-2} \quad (62)$$

B. Chiral anomaly and instanton zero modes

It was well understood already in 1970's that instantons provide an example of explicit violation of the $U_A(1)$ chiral symmetry. The divergence of the corresponding axial current is proportional to the topological charge density $G\tilde{G}$, which in turn is a divergence of the topological Chern-Simons current. Thus the axial charge of fermions, or the number of right minus left-polarized quarks, is intimately related to gauge topology.

How this happens in the instanton case was explained by t' Hooft [18], who found the existence of 4-dimensional bound state, or the *fermion zero mode* of the Dirac operator in the instanton background. Formally it amounts to an additional term in the 4-dimensional quark propagator

$$S(x, y) = \sum_{\lambda} \frac{\psi_{\lambda}(x)\psi_{\lambda}(y)^+}{\lambda + im} \quad (63)$$

with the zero mode $\lambda = 0$. The physical meaning is that the negative energy Dirac sea creates a new state, into which the original quark is pushed into. At the same time, a quark of *opposite chirality* emerges from the Dirac sea as a physical (positive energy) state. The infinite hotel story.

This process can be described by a ‘‘chirality flip’’ of a quark. However, the phenomenon is not reduced just to this: *all* light quark flavors must

experience this together and flip their chiralities *simultaneously*. Because of the Pauli principle, only the zero modes with different flavors can undergo simultaneous tunneling, the t' Hooft effective Lagrangian is therefore a six-quark operator, with $\bar{u}u\bar{d}d\bar{s}s$ quarks. As emphasized by t' Hooft, it is repulsive in the η' channel, and solves the famous the famous $U_A(1)$ problem. But the fact that it is *attractive* in the scalar σ and pseudoscalar π, K, η octet channels leads to even more important consequences, breaking the $SU(N_f)$ chiral symmetry spontaneously [19]. The account for these effects led to the statistical studies of instanton ensembles in the 1990's, for a review see [20]. Many more studies based on these observations, were carried in the last two decades as well: let us just mention our recent study of the so called instanton-sphaleron production process, which can be studied experimentally in colliders [36].

For clarity, let us now discuss some technical issues already discussed in the literature. The first is the explicit analytic form of the 't Hooft operator, which by Fierz transformations, can take several different forms. A straightforward reduction of the product of six unitary color rotation matrices, averaged over the $SU(3)$ group, leads to color structures containing $f^{abc}\lambda^a\lambda^b\lambda^c$ and $d^{abc}\lambda^a\lambda^b\lambda^c$ terms, which is difficult to use in practice. However they (and in fact all color matrices) can be eliminated using specific properties of zero modes producing the following result [58]

$$\begin{aligned} \mathcal{V}_{qqq}^{L+R} = & \frac{G_{Hooft}}{N_c(N_c^2 - 1)} \left[\left(\frac{2N_c + 1}{2(N_c + 2)} \right) \left\| \begin{array}{ccc} \bar{u}_R u_L & \bar{u}_R d_L & \bar{u}_R s_L \\ \bar{d}_R u_L & \bar{d}_R d_L & \bar{d}_R s_L \\ \bar{s}_R u_L & \bar{s}_R d_L & \bar{s}_R s_L \end{array} \right\| \right. \\ & \left. - \frac{1}{2(N_c + 1)} \sum_{a=1}^3 \left(\left\| \begin{array}{ccc} \bar{u}_R \sigma^a u_L & \bar{u}_R \sigma^a d_L & \bar{u}_R s_L \\ \bar{d}_R \sigma^a u_L & \bar{d}_R \sigma^a d_L & \bar{d}_R s_L \\ \bar{s}_R u_L & \bar{s}_R d_L & \bar{s}_R s_L \end{array} \right\| + \left\| \begin{array}{ccc} \bar{u}_R \sigma^a u_L & \bar{u}_R d_L & \bar{u}_R \sigma^a s_L \\ \bar{d}_R u_L & \bar{d}_R d_L & \bar{d}_R s_L \\ \bar{s}_R \sigma^a u_L & \bar{s}_R d_L & \bar{s}_R \sigma^a s_L \end{array} \right\| + \left\| \begin{array}{ccc} \bar{u}_R u_L & \bar{u}_R d_L & \bar{u}_R s_L \\ \bar{d}_R u_L & \bar{d}_R \sigma^a d_L & \bar{d}_R \sigma^a s_L \\ \bar{s}_R u_L & \bar{s}_R \sigma^a d_L & \bar{s}_R \sigma^a s_L \end{array} \right\| \right) \right] \\ & + (L \leftrightarrow R) \end{aligned} \quad (64)$$

with the strength of the 6-q operator

$$G_{Hooft} = \frac{n_{I+\bar{I}}}{2} \left(4\pi^2 \rho^3 \right)^3 \left(\frac{1}{m_u^* \rho} \right) \left(\frac{1}{m_d^* \rho} \right) \left(\frac{1}{m_s^* \rho} \right) \quad (65)$$

with the effective quark masses m_q^* to be explained a bit later.

In (64) all quarks and antiquarks have opposite

chiralities. In a completely massless theory we cannot have ‘‘loop’’ quarks by a propagator conserving chirality. However, the spontaneous breaking of chiral symmetry in the QCD vacuum leads to nonzero quark condensates $\langle \bar{q}_f q_f \rangle \neq 0$. This fact leads to ‘‘dimensional reduction’’ of the six-quark operator to four (and even two-) quark expressions, by ‘‘looping’’

some quark-antiquark pairs into the corresponding condensates. For example, strange quark loops gen-

erate an effective ud -interaction. It also has a structure of two-by-two determinants, which (with some abuse of notations) we write as

$$\mathcal{V}_{qq}^{L+R} = \kappa_2 A_{2N} \left(\det(UD) + B_{2N} \det(U_{\mu\nu} D_{\mu\nu}) \right) + (L \leftrightarrow R) \quad (66)$$

with

$$A_{2N} = \frac{(2N_c - 1)}{2N_c(N_c^2 - 1)} \quad B_{2N} = \frac{1}{4(2N_c - 1)} \quad (67)$$

The coefficient

$$\kappa_2 = 3! G_{\text{Hooft}} \langle \bar{s}_R s_L \rangle = 3 G_{\text{Hooft}} \langle \bar{s} s \rangle < 0 ,$$

is negative and thus attractive. In the Weyl basis, $\sigma_{\mu\nu} \rightarrow i\eta_{\mu\nu}^a \sigma^a$ with the 't Hooft symbol satisfying $\eta_{\mu\nu}^a \eta_{\mu\nu}^b = 4\delta^{ab}$, and (66) can be simplified further

$$\mathcal{V}_{qq}^{L+R} = \kappa_2 A_{2N} \left(\det(UD) - 4B_{2N} \det(U^a D^a) \right) + (L \leftrightarrow R) \quad (68)$$

Another possible “looping” of quarks is possible if we account for nonzero quark masses, in particular the largest strange quark mass m_s . As a result, the effective ud interaction (containing the m_s term) is *stronger* than us, ds interactions, as they only contain negligibly small light quark masses. As noticed by one of us and Rosner [59], the ratio of the coefficients for light-light and light-strange 4-fermion terms is

$$\frac{G(\bar{u}u\bar{d}d)}{G(\bar{u}u\bar{s}s)} = \frac{m_q^* + m_s}{m_q^*} \approx 1.5 \quad (69)$$

One consequence of this is the relatively large violation of $SU(3)_f$ symmetry. Another is that the 't Hooft-operator-induced spin-dependent forces have flavor ratios similar to the magnetic moment ratios (provided one ignores the difference between the on-shell “constituent quark mass” and the determinantal masses m^* .) Therefore, one cannot trace their origin simply by the mass dependence.

Now let us define m^* in the Lagrangian coefficient, following [60], see also [61–63]. If there is a single instanton in the “empty” vacuum, as considered in the original 't Hooft paper, those are just quark masses m_q . The product of the quark masses is however also present in the instanton density (in this setting), and they all cancel out, leaving a finite Lagrangian even

in the chiral limit $m_q \rightarrow 0$.

In an ensemble of instantons, the quark propagator in the QCD vacuum and restricted to the zero modes, is approximated by the form

$$S(x, y) = S_Z(x, y) + \sum_{I, J} \psi_{0I}^*(x) \left(\frac{1}{T} \right)_{I, J} \psi_{0J}(y) \quad (70)$$

where T_{IJ} denotes the so called “instanton hopping” matrix, constructed out of the Dirac zero modes overlaps between neighboring instantons I, J . Note that it contributes as an *inverse* matrix, as propagators are inverse to Dirac operators. So, when one discusses a process in which both points x, y are inside the same instanton I^* , as per the definition of a hard block, we can restrict the sum to only the term with the zero mode of this very instanton. This leads to the following re-definition of the “determinantal mass”

$$\frac{1}{m_u} \equiv \left\langle \left(\frac{1}{T} \right)_{I^* I^*} \right\rangle \quad (71)$$

Furthermore, in the diagrams containing *two* quark propagators of *different flavors* one has a different averaging

$$\frac{1}{m_{uudd}^2} \equiv \left\langle \left(\frac{1}{T} \right)_{I^* I^*}^2 \right\rangle \quad (72)$$

These two quantities were evaluated in the random and interacting instanton liquid model, with

$$\frac{1}{m_u^2} \approx \frac{1}{(177 \text{ MeV})^2} \ll \frac{1}{m_{uudd}^2} \approx \frac{1}{(103 \text{ MeV})^2} \quad (73)$$

The chief consequence of these substantial deviations from mean field can be captured by a “t Hooft operator enhancement factor”

$$f_{\text{tHooft}} \equiv \left(\frac{m_u}{m_{uudd}} \right)^2 \approx 3 \quad (74)$$

This enhancement of 4-fermion operator relative to 2-fermion squared has also been observed on the lattice in [23].

C. Spin and flavor-dependent interactions from zero-modes

Since the t' Hooft induced interaction is non-local, there are additional contributions besides the local terms retained earlier. More specifically, for two flavors its generic form is

$$\begin{aligned} \mathcal{L} = & \kappa_2 A_{2N} \int \prod_{i=1}^4 \frac{d^4 k_i}{(2\pi)^4} \left(\frac{M(k_i)}{M(0)} \right)^{\frac{1}{2}} (2\pi)^4 \delta^4(k_1 + k_3 - k_2 - k_4) \\ & \times \frac{1}{2} \epsilon^{f_1 f_2} \epsilon^{g_1 g_2} \left(\bar{\psi}_{Rf_1}(k_1) \psi_{Lg_1}(k_2) \bar{\psi}_{Rf_2}(k_3) \psi_{Lg_2}(k_4) - 4B_{2N} \bar{\psi}_{Rf_1}(k_1) \sigma^a \psi_{Lg_1}(k_2) \bar{\psi}_{Rf_2}(k_3) \sigma^a \psi_{Lg_2}(k_4) \right) + (L \rightarrow R) \end{aligned} \quad (75)$$

with form-factors, from a Fourier transform of the quark zero mode

$$\frac{M(k)}{M(0)} = \left(2z \left[I_0(z) K_1(z) - I_1(z) K_0(z) - \frac{1}{z} I_1(z) K_1(z) \right] \right)_{z=k\rho/2}^2 \quad (76)$$

We note that the antisymmetric operator for flavor exchange can be rewritten as

$$\epsilon^{f_1 f_2} \epsilon^{g_1 g_2} = \frac{1}{2} \left(\delta^{f_1 g_1} \delta^{f_2 g_2} - \tau^a{}_{f_1 g_1} \tau^a{}_{f_2 g_2} \right) \rightarrow \frac{1}{2} (1 - \tau_1 \cdot \tau_2) \quad (77)$$

so that (75) reads

$$\begin{aligned} \mathcal{L} = & \frac{1}{2} \kappa_2 A_{2N} \int \prod_{i=1}^4 \frac{d^4 k_i}{(2\pi)^4} \left(\frac{M(k_i)}{M(0)} \right)^{\frac{1}{2}} (2\pi)^4 \delta^4(k_1 + k_3 - k_2 - k_4) \\ & \left[\left(\bar{\psi}(k_1) \psi(k_2) \bar{\psi}(k_3) \psi(k_4) + \bar{\psi}(k_1) \gamma_5 \psi(k_2) \bar{\psi}(k_3) \gamma_5 \psi(k_4) \right. \right. \\ & \left. \left. - \bar{\psi}(k_1) \tau^a \psi(k_2) \bar{\psi}(k_3) \tau^a \psi(k_4) - \bar{\psi}(k_1) \tau^a \gamma_5 \psi(k_2) \bar{\psi}(k_3) \tau^a \gamma_5 \psi(k_4) \right) \right. \\ & \left. - 4B_{2N} \left(\bar{\psi}(k_1) \sigma^a \psi(k_2) \bar{\psi}(k_3) \sigma^a \psi(k_4) + \bar{\psi}(k_1) \sigma^a \gamma_5 \psi(k_2) \bar{\psi}(k_3) \sigma^a \gamma_5 \psi(k_4) \right. \right. \\ & \left. \left. - \bar{\psi}(k_1) \sigma^a \tau^b \psi(k_2) \bar{\psi}(k_3) \sigma^a \tau^b \psi(k_4) - \bar{\psi}(k_1) \sigma^a \tau^b \gamma_5 \psi(k_2) \bar{\psi}(k_3) \sigma^a \tau^b \gamma_5 \psi(k_4) \right) \right] \end{aligned} \quad (78)$$

Going ahead of ourselves, we note that in the sequel on the light-front Hamiltonian, we

will use this operator with light cone kinematics, *ultrarelativistic* on-shell spinor, in spin or chiral ba-

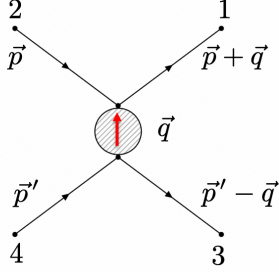


FIG. 15. Kinematics in the center of mass frame of the two-flavor instanton induced interaction with in-out on-shell Dirac fermions.

sis. In this paper, however, we are in the center of mass frame, in the non-relativistic setting of a constituent quark model. Therefore, we perform the non-relativistic reduction of (78) with on-mass-shell normalized Dirac spinors

$$U_s(p) = \begin{pmatrix} f(p)\chi_s \\ g(p)\sigma \cdot p\chi_s \end{pmatrix} \quad V_s(p) = \begin{pmatrix} g(p)\sigma \cdot p\chi_s^C \\ f(p)\chi_s^C \end{pmatrix} \quad (79)$$

with standard normalization factors

$$f(p) = \left(\frac{E_p + m}{2E_p} \right)^{\frac{1}{2}} = (E_p + m)g(p) \quad (80)$$

and $E_p = (p^2 + m^2)^{\frac{1}{2}}$. For the reduction to central, spin-orbit and spin-spin interactions, we set the kinematics in the center of mass defined in Fig. 15 with $k_1 = (E_{p+q}, \vec{p} + \vec{q})$, $k_2 = (E_p, \vec{p})$, $k_3 = (E_{p'-q}, \vec{p}' - \vec{q})$, $k_4 = (E_{p'}, \vec{p}')$, insert (79) into (78) and expand up to order p^2/m^2 . Recall that in a meson state $\bar{q}q$, the labels in Fig. 15 refers also to the flavor and spin $1, 2 \rightarrow U$ with mass m_Q for the quark, and

$3, 4 \rightarrow V$ with mass $m_{\bar{Q}}$ for the anti-quark. More specifically after setting $m = m_Q = m_{\bar{Q}}$, the order q^0/m^0 amounts to the two-body central and spin-spin operators

$$-\frac{1}{4}|\kappa_2|A_{2N} \left(1 - \tau_1 \cdot \tau_2\right) \left(1 - 16B_{2N}\vec{S}_1 \cdot \vec{S}_2\right) \quad (81)$$

in the U(1) or η' channel. For clarity, the form factor is temporarily set to 1 (zero size approximation). Taking into account the overall negative sign in κ_2 , and $16B_{2N} = 4/5$, and the values of $\vec{S}_1 \cdot \vec{S}_2 = -3/4$ for $S = 0$ states, one finds that the last bracket simplifies to $-8/5$ for the pseudoscalar (pion) channel. Note that (78) is only active in the $(\sigma, \pi, \sigma_5, \pi_5, \eta')$ channels. (78) does not contribute to the vector channels.

The relativistic correction $\sim q^2/m^2$ amounts to the two-body operators (with again the form factor set to 1)

$$-\frac{1}{4}|\kappa_2|A_{2N} \left(1 - \tau_1 \cdot \tau_2\right) \left(\frac{1}{4m^2}\right) \left(-L_S - 4S_T + 4B_{2N}(3L_S + 4S_T + 8q^2S_1 \cdot S_2)\right) \quad (82)$$

with spin-orbit and tensor operators

$$L_S = (S_1 + S_2) \cdot (iq \times (p - p')) \quad (83)$$

$$S_T = S_1 \cdot qS_2 \cdot q, \quad S_{12} = 3(S_1\hat{q})(S_2\hat{q}) - (S_1S_2)$$

with L_S symmetrized using $\vec{p} + \vec{p}' = 0$. The translation $iq \rightarrow \nabla$ to configuration space will be understood.

D. Zero-mode-induced potential for pions

In section IV A we have already studied the pion case, and defined the value of the 't Hooft effective coupling (62) needed to put the pion at the empirical mass. The first question we now discuss is whether the ILM (component of the instanton ensemble) can provide a coupling of this magnitude. The answer to this question is affirmative.

The “determinantal masses” induced by the quark condensates are given by the following expressions for light and strange quarks

$$m_q^* = \frac{2\pi^2\rho^2}{3}|\langle\bar{q}q\rangle|, \quad m_s^* = \frac{2\pi^2\rho^2}{3}|\langle\bar{s}s\rangle| + m_s \quad (84)$$

Using them, for a fixed instanton radius $\rho = 0.33 \text{ fm} \approx 1.4 \text{ GeV}^{-1}$, we get the following value of the coupling of $\bar{u}d\bar{d}u$ 't Hooft vertex

$$G_{ud} = A_{2N} \frac{3n}{8} \frac{(4\pi^2)^3 \rho^9}{(m_q^* \rho)^2 (m_s^* \rho)} |\langle \bar{s}s \rangle| \approx 27 \text{ GeV}^{-2} \quad (85)$$

It is larger than the value of 17 GeV^{-2} we fitted from the pion mass using the Schroedinger equation above, by about 50%. However, note that it contains a large (sixth) power of the instanton size, which is not yet defined with sufficiently high precision. The numbers would match if one reduces it from $1/3 \text{ fm}$ to 0.29 fm .

Now, assuming that the 't Hooft-induced potential puts the pion at the right mass, we now turn our attention to the ρ meson. In the previous section we have found that there is an attractive 't Hooft-induced potential which, at the leading non-relativistic order (81), is just a *half* of that for the pion. Naively, one might think that this potential will pull the mass of the ρ to *half* of what it does to the pion, putting it right at the experimentally observed value. Unfortunately, it is not the case. The effects of the 't Hooft operator are too large to be treated as small perturbations. A factor two difference in a potential, does not imply a factor two in the energy, because the wave function itself depends strongly on it. What we found is that, due

to the 't Hooft-induced potential, the pion's size get reduced, making it comparable to the instanton potential range $\sim \rho$. Half of it, acting against the repulsive $V_{SS(r)}$ from the earlier contributions, fail to shrink the ρ size, which remains roughly twice the size of π . This reduces the wave function at small distances roughly by a factor of 2^3 , and effectively reduces the matrix element of the $V^{\text{Hooft}}(r)$ in the ρ case by a comparable factor. The corresponding potentials and wave functions are shown in Fig.16.

E. The ρ meson and the “molecule-induced” potential

This leaves us with the model prediction for the ρ meson mass m_ρ in the vicinity of the mass following from a “generic Cornell meson”, with $m \approx 1.4 \text{ GeV}$, far from its experimental mass. The theory part is missing something very important for the vector light quark channel.

Fortunately, there is still one more effect, already discussed in the literature, the second-order 't Hooft effective forces due to “molecular” configurations, see the lower plot in the Introduction, Fig.1 . In particular, the effective Lagrangian induced by these molecules was used in the theory of color superconductivity at high density [64], from which we borrow its analytic form

$$L_{\text{mol}}/G_{\text{mol}} = \frac{1}{N_c^2} [(\bar{\psi}\gamma_\mu\psi)^2 + (\bar{\psi}\gamma_\mu\gamma_5\psi)^2] - \frac{1}{2N_c(N_c - 1)} [(\bar{\psi}\gamma_\mu\lambda^a\psi)^2 + (\bar{\psi}\gamma_\mu\gamma_5\lambda^a\psi)^2] - \frac{1}{N_c^2} [(\bar{\psi}\gamma_\mu\psi)^2 - (\bar{\psi}\gamma_\mu\gamma_5\psi)^2] - \frac{2N_c - 1}{2N_c(N_c^2 - 1)} [(\bar{\psi}\gamma_\mu\lambda^a\psi)^2 - (\bar{\psi}\gamma_\mu\gamma_5\lambda^a\psi)^2] \quad (86)$$

It follows by using the same color orientation for the instanton and anti-instanton, which locks them to their most attractive channel. The quark fields come from zero modes of I and \bar{I} , so there is no Pauli principle and the flavors can be both the same or different. Note that in in this case the chiralities of the quarks and antiquarks are the same in each term, which is suitable for the ρ meson channel. Choosing the vector $\gamma_\mu\lambda^a$ terms and reducing the color matrices for the meson case, we can reduce it to

$$L_{\text{mol}} = G_{\text{mol}} (\bar{u}\gamma_\mu u)_x (\bar{d}\gamma_\mu d)_y F_{\text{mol}}(x - y) \quad (87)$$

where we introduced another form-factor to account for the nonlocality of the instanton-antiinstanton molecule. In principle, one can evaluate (87) in a way that is analogous to our treatment of the 't Hooft Lagrangian. However, it would now include *two* 4-dimensional integrations over positions of both centers, plus the relatively complicated $I\bar{I}$ interaction depending on the relative color orientations. Qualitatively, one expects its non-locality size to approximately double, so we may just substitute

the instanton size $\rho \rightarrow 2\rho$ in the instanton form factor as an estimate. As a result, its coefficient is reduced by $1/2^3$ in the formfactor (C1). Such a size reduction of the potential range is precisely what is needed to obtain the correct ρ meson mass.

More specifically, setting the corresponding potential into the Schroedinger equation, along with the Cornell and spin-spin terms, we find that the correct ρ mass is indeed obtained for

$$\frac{G_{\text{mol}}}{G_{\text{Hoof}}t} = \frac{120 \text{ GeV}^2}{17 \text{ GeV}^2} \sim \frac{n_{\text{mol}} + n_{\text{ILM}}}{n_{\text{ILM}}} \approx 7 \quad (88)$$

Note that this ratio of couplings (or densities) agrees well with what was deduced from the central potential fitting the linear potential discussed above.

(As a parting comment, we remind the reader that the NJL model – the pioneering effort to de-

scribe chiral symmetry breaking and nonperturbative interactions in hadrons – involves flavor-diagonal terms like the one we used here. In later papers based on the NJL model, those contributions were attributed to the “strong coupling part” of one gluon exchange.)

F. Zero mode effects in heavy-light systems

The spin interactions for heavy-light quarks split into the contributions solely from the non-zero modes which give rise to the same general spin dependent interactions as in (39).

For simplicity, we start with the heavy-light mesons, with a single light quark. The contributions to the quark propagators come from the zero-mode for the light quark, and the non-zero-modes for the heavy-quark. The resulting spin-independent interaction was derived in [58]

$$\mathcal{L}_{qQ} = - \left(\frac{\Delta m_Q \Delta m_q}{2nN_c} \right) \left(\bar{\mathbf{Q}} \frac{1 + \gamma^0}{2} \mathbf{Q} \bar{\mathbf{q}} \mathbf{q} + \frac{1}{4} \bar{\mathbf{Q}} \frac{1 + \gamma^0}{2} \lambda^a \mathbf{Q} \bar{\mathbf{q}} \lambda^a \mathbf{q} \right) \quad (89)$$

while the spin-dependent interaction is more suppressed

$$\mathcal{L}_{qQ}^{\text{spin}} = - \left(\frac{\Delta m_Q^{\text{spin}} \Delta m_q}{2nN_c} \right) \times \frac{1}{4} \left(\bar{\mathbf{Q}} \frac{1 + \gamma^0}{2} \lambda^a \sigma^{\mu\nu} \mathbf{Q} \bar{\mathbf{q}} \lambda^a \sigma^{\mu\nu} \mathbf{q} \right)$$

with $\Delta m_Q^{\text{spin}}/\Delta m_q \sim 1/100$ (charm). The local potential stemming from (89-90) is

$$V_{qQ}(r) = \left(\frac{\Delta m_Q \Delta m_q}{2nN_c} \right) \left(1 + \frac{1}{4} \lambda_q^a \lambda_Q^a \right) \delta^3(r) \quad (90)$$

In the mesons, the colors on the two lines are opposite and the second term dominates the first, so this local potential is negative. For the D meson it amounts to $\langle V_{qQ} \rangle \approx -180 \text{ MeV}$ [58], to be compared with the non-relativistic energy due to the standard Hamiltonian, kinetic plus central potential average

$$\langle P^2/2m_q + V_c(r) \rangle \approx +250 \text{ MeV}.$$

The spin-spin potential is

$$V_{qQ}^{\text{spin}}(r) = - \left(\frac{\Delta m_Q^{\text{spin}} \Delta m_q}{2nN_c} \right) S_q \cdot S_Q \lambda_q^a \lambda_Q^a \delta^3(r) \quad (91)$$

For the D meson both the relative spin and color are negative, so the contribution of this term is negative as well, giving $\langle V_{qQ}^{\text{spin}} \rangle \approx -42 \text{ MeV}$ [58]. The contribution of this term to the spin splitting is then

$$M(D^*) - M(D) = (4/3)42 \text{ MeV} = 56 \text{ MeV}$$

to be compared with our calculations above giving together $\langle V_{SS}^{\text{pert}} + V_{SS}^{\text{inst}} \rangle \approx 96 \text{ MeV}$. We thus conclude that all the three contributions together – the perturbative one and the two instanton-induced ones – do finally reproduce this mass difference, close to the experimental value $M(D^*) - M(D) = 137 \text{ MeV}$.

V. SUMMARY AND DISCUSSION

The purpose of this work was to have a fresh look at the origins of the central and spin-dependent potentials, used in the non-relativistic description of mesons. We focused in the range of “intermedi-

ate distances” $r \sim 0.2 - 0.5$ fm, where the spin-dependent forces are mostly active.

The phenomenological part of this paper focused solely on mesons, from heavy charmonia to heavy-light and to light-light ones. Using data for the spin splittings in the 1S shell (2 states) and the 1P shell (4 states), we evaluated matrix elements of the individual spin-dependent potentials. Among the important observations is a change of sign of the tensor force for lighter systems.

The theory part started with a reformulation of the instanton ensemble. Unlike previous studies using the dilute ILM, and mostly focused on the spontaneous breaking of chiral symmetry and zero modes, the ensemble we consider now includes $I\bar{I}$

”molecules”. It was shown that in this regime the instanton-induced potential reproduces the magnitude of the central potential, up to distances $r < 1$ fm. Ascribing the central potential $V_C(r)$ at $r < 1$ fm to this extra contribution, we get its normalization fixed. It turns out to be about twice less dense than the lattice extrapolations of Fig. 4(b), with a diluteness parameter $\kappa \sim 1$.

This leads to evaluations of the nonperturbative part of spin-dependent potentials. Their application to heavy-heavy systems can be considered consistent with available lattice data for $V_{SS}(r)$, and also with phenomenology. One important finding is that the perturbative and instanton-induced contributions are *comparable in magnitude*. Together they semi-quantitatively reproduce lattice-based potential and the spin splitting in heavy quarkonia.

Going further from heavy to light systems, we analyzed four P-shell states, attempting to extract spin-orbit and tensor potentials. The reader should however be aware that for light quarks, we no longer are well below the open decay channels, whose possible effects on observed masses have been ignored for now. Experience with some mesons in the past suggests that these effects are small. An argument that we mostly have it correct is that, as one can see from Table III, that for all three potentials the trend, from heavy to light quarks, seems to be consistent.

Although our straightforward evaluation of perturbative and instanton-induced potentials have not reproduced the apparently negative tensor force for light quarks, the negative *sign* of the instanton-induced term indicates that, with some play of parameters, it perhaps can be done.

Furthermore, for light quarks there exists “anomalous” processes, in which quarks do not travel continuously in time, but are instead dumped into the Dirac sea and substituted by another quark, with different value of the chirality. The non-relativistic reduction of 6-quark ’t Hooft operator have produced novel spin-dependent forces. Their application to the pion case is successful, as well as to the heavy-light systems. The effects related to the zero modes and the ’t Hooft effective interactions can still be put in the form of quasi-local flavor-nondiagonal potentials, i.e. central and spin-dependent. The phenomenological implications of this is a reminder of the *two component* instanton model discussed here, meaning that for the ’t Hooft potential the instanton density is the smaller one, taken from the original ILM. The magnitude of such ’t Hooft poten-

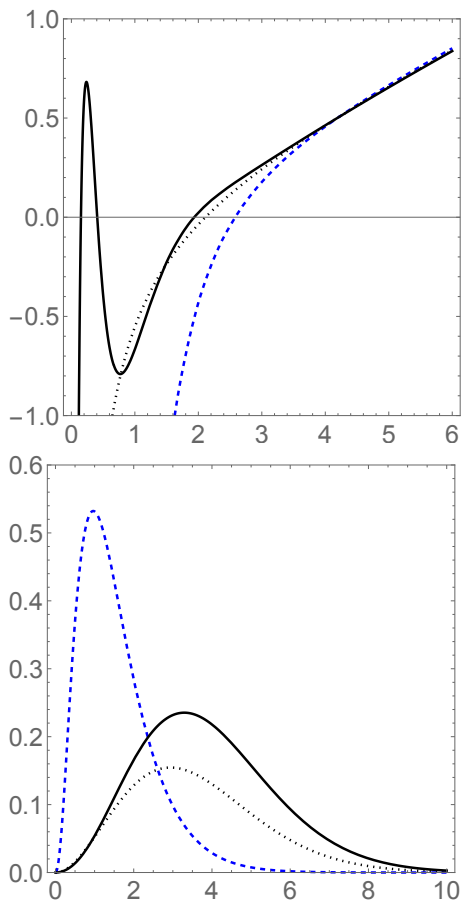


FIG. 16. The total potentials including the ’t Hooft ones (upper plot) and wave functions as $r^2 \psi(r)^2$ (lower plot) for the ρ channel (solid curves), the π channel (blue dashed curves) and the generic Cornell potential (black dots). All potentials are shown versus the distance r in GeV^{-1} .

tial is found of the size needed to put the pion mass at its small physical value. It is in agreement with the long-known view of the pion as depicted in the upper Fig. 1.

The case of the ρ meson is more complicated. Even with the 't Hooft potential its mass remains well above the observed value. However, there is the so called “molecular” component, schematically shown in the lower part of Fig. 1. It generates attractive forces diagonal in chirality. Assuming that with the molecular component the density is 7 times larger than that of the original ILM, we get an estimate of its coupling which we find to put the ρ meson in the correct mass range.

The focus of this work has not been on numerical accuracy, but rather on the microscopic origin of the central and spin-dependent forces. It should be viewed as an introduction to the use of these concepts for the light front Hamiltonians and wave functions, which we will address next.

In sum, the paper proposes novel interpretations of interquark potentials, that should and will be tested. One way to do this is to calculate all spin-

dependent potentials on the lattice *during* a “cooling” process (e.g. via gradient flow), and assess how the results depend on the cooling time (resolution). This will allow for a quantitative discrimination between the perturbative (gluon-induced), and topological (instanton-induced) effects, at low resolution.

VI. ACKNOWLEDGEMENTS

This work was supported by the U.S. Department of Energy under Contract No.DE-FG-88ER40388.

Appendix A: Asymptotics of $V_C(r)$

The instanton induced central potential $V_C(r)$ in Fig. 5 asymptotes twice the self-energy $2\Delta m_Q$. This asymptotics is reached from *above* in singular gauge contrary to expectations. The simplest way to see this, is to note that

$$2\Delta M_{Q\rho} = \frac{8\pi n\rho^4}{N_c} \int_0^\infty dy y^2 \left(1 + \cos\left(\frac{\pi y}{\rho^2 + y^2}\right) \right) \approx \frac{8\pi n\rho^4}{N_c} 2.2 \quad (\text{A1})$$

is substantially smaller than the potential in Fig. 5. A numerical evaluation of $I(x)$ as in (18) at large x , is shown in Fig. 17. It confirms that the asymptotics is slowly reached from above.

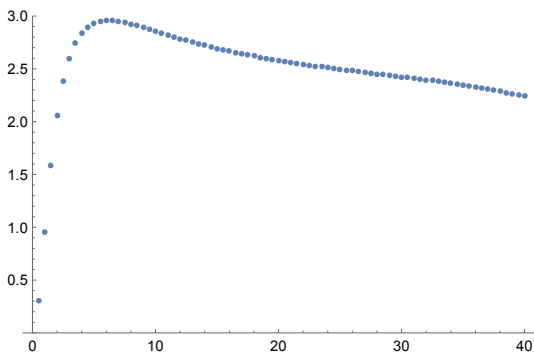


FIG. 17. $I(x)$ versus x as given in (5)

We note that a Taylor expansion of the integrand in $I(x)$ suggests $1/r^3$ as the leading contribution, but the remaining integration is divergent, thereby

invalidating the expansion. In [65] it was suggested that the asymptotics is reached from below through $-\pi^2/2r$. This result is correct in a perturbative regular gauge with no additional color rotations, but not in a non-perturbative singular gauge with additional color rotations. Also, the $1/r$ central potential yields a spin-spin potential $V_{SS}(r)$ as a delta-function which is also not compatible with the $1/r^2$ behavior noted above. Fig. 17 can be fitted numerically by $2\Delta M_Q + C/r^p$ with $p \ll 1$ and $C > 0$. Its ensuing Laplacian then gives $p(1-p)/r^{2+p}$, which is consistent with $V_{SS}(r)$ at large r .

Appendix B: Definitions of the spin-dependent potentials

Following Ref. [7], we give for completeness the correlation functions generating the five spin-dependent potentials. The integrals over points z, z' are taken along two Wilson lines located at \vec{x}_1, \vec{x}_2 and running in the Euclidean time direction, from

$-T/2$ to $T/2$. The limit of large $T \rightarrow \infty$ is not written explicitly but assumed. The normalization to

$\langle 1 \rangle$ means subtraction of the central potential coming from the correlator of Wilson lines without the extra field strengths

$$\begin{aligned} \frac{r^k}{r} \frac{dV_1(r)}{dr} &= \epsilon_{ijk} \int dz dz' \left(\frac{z-z'}{T} \right) \frac{g^2}{2} \langle B^i(\vec{x}_1, z) E^j(\vec{x}_1, z') \rangle / \langle 1 \rangle \\ \frac{r^k}{r} \frac{dV_2(r)}{dr} &= \epsilon_{ijk} \int dz dz' \left(\frac{z-z'}{T} \right) \frac{g^2}{2} \langle B^i(\vec{x}_2, z) E^j(\vec{x}_1, z') \rangle / \langle 1 \rangle \\ &\times [(\hat{r}^i \hat{r}^j - \delta_{ij}/3) V_3(r) + \delta_{ij}/3 V_4(r)] = \int dz dz' \frac{g^2}{T} \langle B^i(\vec{x}_2, z) E^j(\vec{x}_1, z') \rangle / \langle 1 \rangle \end{aligned} \quad (\text{B1})$$

Although it involves only the vector product of electric and magnetic fields, using the Bianchi identity one can express it via a correlator of two B fields, as expected for non-relativistic spin interactions. It is however of little importance for instantons, which

are (anti) self-dual $\vec{E} = \pm \vec{B}$.

Note that the reduction of the dressed Wilson line “WEW” line with an electric field insertion can be made into a derivative of the Wilson line over its location, via the following steps

$$\begin{aligned} &D_m(y) \mathbf{W}(x_0, y_0) - \mathbf{W}(x_0, y_0) D_m(y) \\ &= \langle x_0 | D_0 \frac{1}{iD_0} - \frac{1}{iD_0} D_m | y_0 \rangle \\ &= \langle x_0 | \frac{1}{iD_0} [iD_0, D_m] \frac{1}{iD_0} | y_0 \rangle \\ &= \langle x_0 | \frac{1}{iD_0} (-F_{0m}) \frac{1}{iD_0} | y_0 \rangle = \int_{-\frac{1}{2}T}^{+\frac{1}{2}T} dz_0 \mathbf{W}(-T, z_0) (-F_{0m})(z_0) \mathbf{W}(z_0, T) \end{aligned} \quad (\text{B2})$$

and in the large $|T| \rightarrow \infty$ asymptotic the field is assumed to vanish, so the covariant derivative can be changed to ordinary one.

Subsequent discussions of the $\mathcal{O}(1/m^2)$ of the potentials have been made, starting from complete effective actions of NRQCD and pNRQCD to this order, and some modifications of the expressions in [7] were found (See Eqs. 49-51 in [1]). Modulo matching, the only difference was noted in the spin-orbit coefficient with no $\frac{1}{2}$ in (B1). However, for the purposes of our work, it is enough to note that the spin-spin and spin-orbit potentials are related to the correlators of two magnetic fields, and the spin-orbit to the correlator of electric and magnetic fields. (Of course, the correlators include the appropriate Wilson lines, and are integrated over the time difference

between the field strengths.)

Appendix C: Form-factor in the 't Hooft Lagrangian

In many applications, the instanton induced form-factor on the tunneling quarks, is used in the momentum representation. More specifically, as the Fourier transform of the zero modes in (76). However, in the effective potential we use, there are four zero modes, thus the fourth power of $M(k)$. Its inverse Fourier transform to coordinate space is complicated. We use instead directly the coordinate expression, with two *densities* of zero modes separated by a distance r , with the explicit integration over the location of the instanton center z_μ

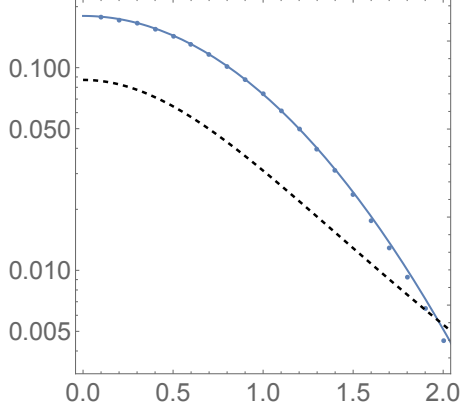


FIG. 18. Numerically integrated and normalized integral (C1) (points), compared to a fit (solid line). Also for comparison we show (the dashed line), the normalized “smoothed delta function” as used in (48) for $\delta = \rho$. It was our initial choice, but as shown here, it does not provide an accurate description of the form-factor and therefore is not used.

$$F(r) \sim \int d^4 z |\psi_0(z^\mu - r^\mu/2)|^2 |\psi_0(z^\mu + r^\mu/2)|^2 \int \frac{z^3 dz \sin^2(\theta) d\theta}{(z^2 + r^2/4 + z r \cos(\theta) + \rho^2)^3 (z^2 + r^2/4 - z r \cos(\theta) + \rho^2)^3} \approx 0.18 \exp(-0.89 r^2) \quad (\text{C1})$$

The last expression is a fit, normalized by $\int d^3 F(r) = 1$, with our standard size $\rho = 1.4 \text{ GeV}^{-1}$. The comparison between the numerical integral and the fit is shown in Fig. 18.

Appendix D: Field strengths through conformal mapping

$$y^2 \vec{E} = \vec{\sigma} \left(f' - \frac{(\vec{y})^2}{y^2} (f' - 2f\bar{f}) \right) + \frac{(\vec{y} \cdot \vec{\sigma} \vec{y} - y_4 \vec{\sigma} \times \vec{y})}{y^2} (f' - 2f\bar{f})$$

$$y^2 \vec{B} = \vec{\sigma} \left(2f\bar{f} + \frac{(\vec{y})^2}{y^2} (f' - 2f\bar{f}) \right) - \frac{(\vec{y} \cdot \vec{\sigma} \vec{y} - y_4 \vec{\sigma} \times \vec{y})}{y^2} (f' - 2f\bar{f}) \quad (\text{D1})$$

with $E^i = F^{i4}$ and $B^i = \frac{1}{2} \epsilon^{ijk} F^{jk}$. For self-dual fields $f' = 2f\bar{f}$ and $\vec{E} = \vec{B}$ are hedgehogs in color-spin as expected for the instanton path. For the sphaleron path, we have $f = \frac{1}{2}$ and $(\vec{E} + \vec{B}) = \vec{\sigma}/2y^2$, as only the electric plus magnetic field sum is hedgehog in color-spin. We then use the conformal (stereographic) map (Step 2), as explained in the text.

The field strengths F_{MN} and its dual $\star F_{MN}$ for the tunneling at fixed energy in $O(4)$ symmetric form (Step 1) are given by

[1] A. Pineda and A. Vairo, *Phys. Rev. D* **63**, 054007 (2001), [Erratum: *Phys.Rev.D* 64, 039902 (2001)],

arXiv:hep-ph/0009145.

- [2] N. Brambilla, G. a. Krein, J. Tarrús Castellà, and A. Vairo, *Phys. Rev. D* **97**, 016016 (2018), [arXiv:1707.09647 \[hep-ph\]](#).
- [3] J. F. Arvis, *Phys. Lett. B* **127**, 106 (1983).
- [4] O. Aharony and N. Klinghoffer, *JHEP* **12**, 058 (2010), [arXiv:1008.2648 \[hep-th\]](#).
- [5] A. Athenodorou and M. Teper, (2021), [arXiv:2106.00364 \[hep-lat\]](#).
- [6] C. G. Callan, Jr., R. F. Dashen, D. J. Gross, F. Wilczek, and A. Zee, *Phys. Rev. D* **18**, 4684 (1978).
- [7] E. Eichten and F. Feinberg, *Phys. Rev. D* **23**, 2724 (1981).
- [8] Y. Nambu and G. Jona-Lasinio, *Phys. Rev.* **122**, 345 (1961).
- [9] M. A. Shifman, A. I. Vainshtein, and V. I. Zakharov, *Nucl. Phys. B* **147**, 385 (1979).
- [10] V. A. Novikov, M. A. Shifman, A. I. Vainshtein, and V. I. Zakharov, *Nucl. Phys. B* **191**, 301 (1981).
- [11] E. V. Shuryak, *Rev. Mod. Phys.* **65**, 1 (1993).
- [12] A. A. Belavin, A. M. Polyakov, A. S. Schwartz, and Y. S. Tyupkin, *Phys. Lett. B* **59**, 85 (1975).
- [13] E. V. Shuryak, *Nucl. Phys. B* **198**, 83 (1982).
- [14] D. B. Leinweber, in *Workshop on Light-Cone QCD and Nonperturbative Hadron Physics* (1999) [arXiv:hep-lat/0004025](#).
- [15] J. C. Biddle, W. Kamleh, and D. B. Leinweber, *Phys. Rev. D* **102**, 034504 (2020), [arXiv:1912.09531 \[hep-lat\]](#).
- [16] J. C. Biddle, W. Kamleh, and D. B. Leinweber, *EPJ Web Conf.* **245**, 06010 (2020), [arXiv:2009.12047 \[hep-lat\]](#).
- [17] I. Zahed, *Phys. Rev. D* **104**, 054031 (2021), [arXiv:2102.08191 \[hep-ph\]](#).
- [18] G. 't Hooft, *Phys. Rev. D* **14**, 3432 (1976), [Erratum: *Phys.Rev.D* **18**, 2199 (1978)].
- [19] E. V. Shuryak, *Nucl. Phys. B* **203**, 140 (1982).
- [20] T. Schäfer and E. V. Shuryak, *Rev. Mod. Phys.* **70**, 323 (1998), [arXiv:hep-ph/9610451](#).
- [21] L. Y. Glozman, C. B. Lang, and M. Schrock, *Phys. Rev. D* **86**, 014507 (2012), [arXiv:1205.4887 \[hep-lat\]](#).
- [22] M. C. Chu, J. M. Grandy, S. Huang, and J. W. Negele, *Phys. Rev. D* **49**, 6039 (1994), [arXiv:hep-lat/9312071](#).
- [23] P. Faccioli and T. A. DeGrand, *Phys. Rev. Lett.* **91**, 182001 (2003), [arXiv:hep-ph/0304219](#).
- [24] D. M. Ostrovsky, G. W. Carter, and E. V. Shuryak, *Phys. Rev. D* **66**, 036004 (2002), [arXiv:hep-ph/0204224](#).
- [25] F. R. Klinkhamer and N. S. Manton, *Phys. Rev. D* **30**, 2212 (1984).
- [26] E.-M. Ilgenfritz and E. V. Shuryak, *Nucl. Phys. B* **319**, 511 (1989).
- [27] R. Rapp, T. Schäfer, E. V. Shuryak, and M. Velkovsky, *Phys. Rev. Lett.* **81**, 53 (1998), [arXiv:hep-ph/9711396](#).
- [28] E. Shuryak and I. Zahed, *Phys. Rev. D* **103**, 054028 (2021), [arXiv:2008.06169 \[hep-ph\]](#).
- [29] Y. Liu and I. Zahed, (2021), [arXiv:2102.07248 \[hep-ph\]](#).
- [30] E. V. Shuryak, *Nucl. Phys. B* **302**, 621 (1988).
- [31] I. I. Balitsky and A. V. Yung, *Phys. Lett. B* **168**, 113 (1986).
- [32] A. V. Yung, *Nucl. Phys. B* **297**, 47 (1988).
- [33] J. J. M. Verbaarschot, *Nucl. Phys. B* **362**, 33 (1991), [Erratum: *Nucl.Phys.B* **386**, 236–236 (1992)].
- [34] V. V. Khoze and A. Ringwald, (1991).
- [35] E. V. Shuryak and J. J. M. Verbaarschot, *Phys. Rev. Lett.* **68**, 2576 (1992).
- [36] E. Shuryak and I. Zahed, (2021), [arXiv:2102.00256 \[hep-ph\]](#).
- [37] M. Luscher and P. Weisz, *JHEP* **02**, 051 (2011), [arXiv:1101.0963 \[hep-th\]](#).
- [38] A. Athenodorou, P. Boucaud, F. De Soto, J. Rodríguez-Quintero, and S. Zafeiropoulos, *JHEP* **02**, 140 (2018), [arXiv:1801.10155 \[hep-lat\]](#).
- [39] P. Boucaud, F. De Soto, A. Le Yaouanc, J. P. Leroy, J. Micheli, H. Moutarde, O. Pene, and J. Rodríguez-Quintero, *JHEP* **04**, 005 (2003), [arXiv:hep-ph/0212192](#).
- [40] E. V. Shuryak and I. Zahed, *Phys. Rev. D* **62**, 085014 (2000), [arXiv:hep-ph/0005152](#).
- [41] M. Giordano and E. Meggiolaro, *Phys. Rev. D* **78**, 074510 (2008), [arXiv:0808.1022 \[hep-lat\]](#).
- [42] M. Giordano and E. Meggiolaro, *Phys. Rev. D* **81**, 074022 (2010), [arXiv:0910.4505 \[hep-ph\]](#).
- [43] U. T. Yakhshiev, H.-C. Kim, M. M. Musakhanov, E. Hiyama, and B. Turimov, *Chin. Phys. C* **41**, 083102 (2017), [arXiv:1602.06074 \[hep-ph\]](#).
- [44] E. V. Shuryak, *Nucl. Phys. B* **203**, 93 (1982).

- [45] Y. Liu, M. A. Nowak, and I. Zahed, *Phys. Rev. D* **100**, 126023 (2019), arXiv:1904.05189 [hep-ph].
- [46] Y. Liu, M. A. Nowak, and I. Zahed, (2019), arXiv:1909.02497 [hep-ph].
- [47] M. Luscher, *Phys. Lett. B* **70**, 321 (1977).
- [48] B. M. Schechter, *Phys. Rev. D* **16**, 3015 (1977).
- [49] V. A. Rubakov, D. T. Son, and P. G. Tinyakov, *Phys. Lett. B* **287**, 342 (1992).
- [50] D. Gromes, *Z. Phys. C* **26**, 401 (1984).
- [51] W. Buchmuller, *Phys. Lett. B* **112**, 479 (1982).
- [52] R. D. Pisarski and J. D. Stack, *Nucl. Phys. B* **286**, 657 (1987).
- [53] Y. Koma and M. Koma, *Nucl. Phys. B* **769**, 79 (2007), arXiv:hep-lat/0609078.
- [54] T. Kawanai and S. Sasaki, *Phys. Rev. D* **92**, 094503 (2015), arXiv:1508.02178 [hep-lat].
- [55] M. Koma, Y. Koma, and H. Wittig, *PoS LAT2005*, 216 (2006), arXiv:hep-lat/0510059.
- [56] T. Barnes, S. Godfrey, and E. S. Swanson, *Phys. Rev. D* **72**, 054026 (2005), arXiv:hep-ph/0505002.
- [57] J. Koponen, A. C. Zimmermann-Santos, C. T. H. Davies, G. P. Lepage, and A. T. Lytle, *Phys. Rev. D* **96**, 054501 (2017), arXiv:1701.04250 [hep-lat].
- [58] S. Chernyshev, M. A. Nowak, and I. Zahed, *Phys. Rev. D* **53**, 5176 (1996), arXiv:hep-ph/9510326.
- [59] E. V. Shuryak and J. L. Rosner, *Phys. Lett. B* **218**, 72 (1989).
- [60] P. Faccioli and E. V. Shuryak, *Phys. Rev. D* **64**, 114020 (2001), arXiv:hep-ph/0106019.
- [61] H. Forkel and M. Nielsen, *Phys. Lett. B* **345**, 55 (1995), arXiv:hep-ph/9408396.
- [62] A. Blotz and E. V. Shuryak, *Phys. Rev. D* **55**, 4055 (1997), arXiv:hep-ph/9606355.
- [63] V. V. Braguta and A. I. Onishchenko, *Phys. Lett. B* **591**, 255 (2004), arXiv:hep-ph/0311146.
- [64] R. Rapp, T. Schäfer, E. V. Shuryak, and M. Velkovsky, *Annals Phys.* **280**, 35 (2000), arXiv:hep-ph/9904353.
- [65] U. T. Yakhshiev, H.-C. Kim, M. M. Musakhanov, E. Hiyama, and B. Turimov, *Chin. Phys. C* **41**, 083102 (2017), arXiv:1602.06074 [hep-ph].